MEASUREMENTS OF HEAT TRANSFER RATES WITHIN A PLANE SHOCK WAVE USING VERY FINE COLD WIRES

Thesis by

Lieutenant Charles F. Stebbins

United States Air Force

In Partial Fulfillment of the Requirements

For the Degree of

Aeronautical Engineer

California Institute of Technology

Pasadena, California

1963

ACKNOWLEDGMENT

This paper is a result of the efforts of several individuals. The author owes a very special debt of gratitude to Professor Anatol Roshko whose interest and close association in the project brought forth its conclusion.

The use of the 17-inch shock tube was made possible through the instruction and encouragement of Professor Bradford Sturtevant and Mr. Erik Slachmuylders.

The author also wishes to thank Mr. Lewis Balthasar and Mr. Ray Wagoner for their much used technical assistance.

Mrs. Geraldine Krentler produced the typed manuscript from rough notes and is especially thanked for reproducing the photo data contained herein.

ABSTRACT

Preliminary results of measurements of thermal shock structure are presented. Cold wire probes, of the type developed by W. H. Christiansen (Ref. 2), were constructed utilizing wires of .00001" and .00005" diameters. Heat transfer measurements were obtained at $M_s \doteq 5$ and 7.5 in the GALCIT 17-inch shock tube over a range of initial pressures from 25 to 200 μ Hg, producing thicknesses on the order of one centimeter.

The heat transfer data obtained are compared with predictions based on the Navier-Stokes theory and the recent Liepmann-Narasimha-Chahine theory (Ref. 3) for shock profiles and the free molecule heat-transfer theory of Stalder, et al., (Ref. 1).

TABLE OF CONTENTS

LIST OF TABLES AND FIGURES

LIST OF TABLES AND FIGURES (CONTD.)

LIST OF SYMBOLS

a	Speed of sound
c	Specific heat
d	Diameter
E	Voltage
$f^o(s)$, $g^o(s)$	Non-dimensional relations defined in Ref. 1
g	Gram
I	Current
k	Coefficient of thermal conductivity
^oK	Degrees absolute
$K_n = \frac{\Lambda}{d}$	Knudsen number
ℓ	Length
M_s	Mach number of incident shock wave
mv	Millivolt
Nu	Nusselt number
p	Pressure
Q	Heat flux to cylinder
q	Heat flux per unit area and time
R	Electrical resistance in ohms
$s = V_s / v_m$	Molecular speed ratio
t	Dimensional time
Tr	Temperature an unheated wire would reach in equilibrium with the flow (Recovery Temperature)
T	Temperature
v	Velocity in shock tube coordinates
V_s	Velocity of the incident shock wave

LIST OF SYMBOLS (CONTD.)

v_m	Most probable molecular speed
x	Oscillogram abcissa
y	Oscillogram ordinate
α	Temperature coefficient of resistivity
a_z	Accommodation coefficient
ρ	Density
Λ	Mean free path of molecule
Ω	Ohms
μ	Viscosity coefficient
μ sec	Microsecond
μ Hg	Microns of mercury, pressure
σ	Coefficient of electrical resistivity
$\mathcal{T}$	Non-dimensional time

Subscripts

0	Reference level on oscillogram
1	Refers to the initial conditions of the test gas
2	Refers to the conditions in the region behind the incident shock
i	Refers to some initial conditions
r	Refers to recovery conditions

Superscripts

$(\dot{})$	$d(\ )/dt$

I. INTRODUCTION

The GALCIT 17-inch shock tube (Ref. 4) makes it possible to work at initial tube pressures of a few microns of Hg. The low leak rate insures purity of the test gas, and, the large diameter makes it possible to achieve sufficient separation between shock wave and contact surface to give a well-defined shock wave and after-flow. Another, earlier GALCIT development, namely the cold-wire probe (Christiansen, Ref. 2) had the possibilities of sufficient response for making a measurement of shock structure. An investigation of this possibility is the main theme of the present work. Christiansen used wires down to .0001 inch in diameter for studying the flow behind shock waves and indicated that the diameters would have to be much smaller for measurements inside a shock wave, i.e., over much shorter flow durations. In view of some earlier success in mounting and using .00001 inch diameter wires (Ref. 8), it was decided to attempt to use these in the shock tube.

The application of these wires in the shock tube problem is quite different from Sherman's (Ref. 9) technique of measuring the structure of a stationary shock. In the latter case, the wire was allowed to come to equilibrium at each measuring point, and the basis of the measurement was the variation of the equilibrium temperature through the shock. In the shock tube experiment, it is the heat transfer rate that provides the basic measurement and it has to be related to the various parameters of the shock profile.

A further incentive for the present experiments was the recent work on shock structure by Liepmann-Narasimha-Chahine (L-N-C, Ref. 3), which indicates some interesting departures from the Navier-Stokes theory at shock Mach numbers above 2.

II. SHOCK STRUCTURE MEASUREMENTS

A. General Experimental Procedure

A stationary very fine cold wire (Ref. 2) was placed in the GALCIT 17-inch shock tube (Ref. 4). A thick (1 cm) shock was allowed to pass over the wire, heating it. The object of the experiment was to obtain $\dot{E}_w$, the wire response. The response of a cold wire to a shock produces an indirect measurement of shock profile, i.e., the measured $\dot{E}_w$ is related to the distribution of ρ, v, and T within the shock (v in shock tube coordinates).

Heat transfer to a cold wire is proportional to dT/dt, thus to dR/dt and dE/dt in the following manner (Ref. 2):

$$R_w = R_1[1 + \alpha_1(T_w - T_1)] \tag{1}$$

Using Ohm's law:

$$E_w = IR_1[1 + \alpha_1(T_w - T_1)]$$

Differentiating:

$$\dot{E}_w = IR_1\alpha_1\dot{T}_w \tag{2}$$

In region 2 behind the shock, the flow is uniform, providing constant values of $\dot{T}_w$ and $\dot{E}_w$, since the wire is simply a calorimeter gauge. This region of known conditions is used as a

convenient reference. A shock of zero thickness, then, would produce a linear response, while the response to a shock of finite thickness depends on the distribution of ρ, v, and T within the shock (see sketch).

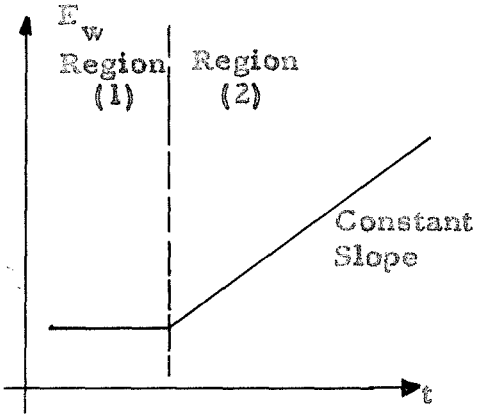

Zero Thickness

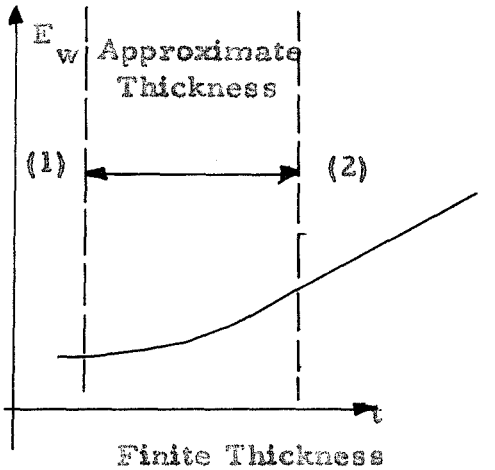

Finite Thickness

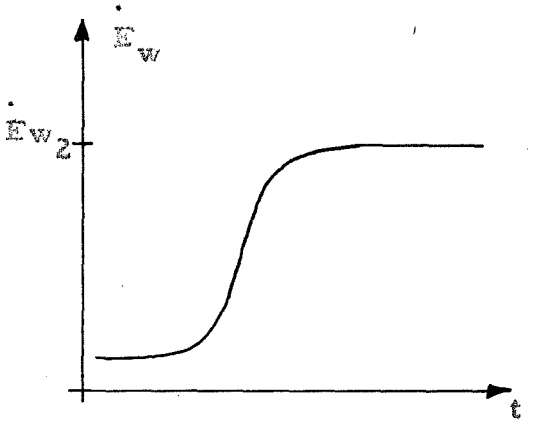

Differentiated Output

B. Theoretical Considerations

The goal of the experiment is to compare the measured E_w and $\dot{E}_w$ with theoretical predictions. To obtain the latter, one uses predicted values of ρ, u, and T in an appropriate heat transfer theory. Flow was, in all cases, free molecule flow for the fine wires used in the experiment (minimum Knudsen number, $\frac{\Delta}{d}$, was 250). Stalder, et al., (Ref. 1) find the following:

$$q_f = \frac{p v_m \alpha_t}{2\pi^{3/2}} \left[\frac{T_1}{T} g^\circ(s) - f^\circ(s) \right] \tag{3}$$

In equation (3), which is an equation for the rate of change of wire conditions, any effects due to radiation and end losses are secondary, due to the short times involved. The molecular speed ratio, s, may be written

$$s = \frac{\sqrt{\frac{\gamma}{2}}\, M_s \left\{ 1 - \frac{\rho_1}{\rho} \right\}}{\sqrt{\frac{T}{T_1}}} \tag{4}$$

Using

$$v_m = \left(\frac{v}{V_s} \right) \left(\frac{V_s}{s} \right) = \left(1 - \frac{\rho_1}{\rho} \right) \frac{V_s}{s}$$

and

$$p = p_1 \left(\frac{\rho}{\rho_1} \right) \left(\frac{T}{T_1} \right)$$

one obtains

$$q_f = \frac{P_1 V_s \alpha_z}{2\pi^{3/2}\sqrt{\frac{\gamma}{2}}\, M_s}\sqrt{\frac{T}{T_1}}\,\frac{\rho}{\rho_1}\left[\frac{T}{T_1}f^\circ(s) - g^\circ(s)\right]$$

$$q_f \equiv B\sqrt{\frac{T}{T_1}}\left(\frac{\rho}{\rho_1}\right)\left(\frac{T}{T_1}f^\circ(s) - g^\circ(s)\right) \tag{5}$$

The calorimeter relation (Ref. 2) is

$$\dot{T}_w = \frac{4}{d\,\rho_w c_w}\, q_f \tag{6}$$

Therefore

$$\dot{T}_w = \frac{4B}{d\,\rho_w c_w}\sqrt{\frac{T}{T_1}}\left(\frac{\rho}{\rho_1}\right)\left(\frac{T}{T_1}f^\circ(s) - g^\circ(s)\right)$$

$$\dot{T}_w \equiv A\sqrt{\frac{T}{T_1}}\left(\frac{\rho}{\rho_1}\right)\left(\frac{T}{T_1}f^\circ(s) - g^\circ(s)\right) \tag{7}$$

Using equation (2),

$$\dot{E}_w = I R_1 \alpha_1 A\sqrt{\frac{T}{T_1}}\left(\frac{\rho}{\rho_1}\right)\left(\frac{T}{T_1}f^\circ(s) - g^\circ(s)\right) \tag{8}$$

A slight modification is presented, governing a

"warm" wire.

$$\dot{E}_w = I R_1 \alpha_1 A \left\{ \sqrt{\frac{T}{T_1}} \left(\frac{\rho}{\rho_1} \right) \left(\frac{T}{T_1} f^\circ(s) - \frac{T_w}{T_1} g^\circ(s) \right) + \left(\frac{T_w}{T_1} - 1 \right) g^\circ(s) \right\} \tag{9}$$

A "warm" wire is one in which the current is high enough to heat it above ambient conditions. (This was necessary to obtain sufficient response (Eq. (2)).)

For an absolute measurement of E_w or $\dot{E}_w$, the wire constants a_1, a_2, d, ρ_w and c_w, must be found. The most accurate method for wire calibration is probably that which uses the response in region (2), since conditions behind the shock are accurately known. This may be accomplished as follows: Resistance is defined as

$$R_1 = \frac{\sigma_1 \ell}{\pi d^2/4} \tag{10}$$

Forced convection heat transfer may be written in terms of Nusselt number,

$$Q_{forced} = \pi \kappa Nu \ell (T_r - T_w) \tag{11}$$

Tr is the recovery temperature of the flow. Combining equations (1), (2), (6), (10), and (11),

$$\frac{\dot{E}}{I} = 4\kappa Nu \left(\frac{\alpha_1}{d^2 \varsigma c}\right)_w R_1 (T_r - T_w) \tag{12}$$

Using the reference region (2) and introducing the Prandtl and Reynolds numbers,

$$\frac{\dot{E}_2 Pr_2 Re_2}{4 c_p (\varsigma u)_2 R_1 Nu_2} = \left(\frac{\alpha_1}{d\varsigma c}\right)_w (T_r - T_1) - \left(\frac{1}{d\varsigma c}\right)_w \left(\frac{R_w}{R_1} - 1\right) \tag{13}$$

This is of the form y = mx + b. Holding appropriate quantities fixed, one may obtain $(\alpha_1/d\rho c)_w$ and $(1/d\rho c)_w$ from two or more experiments. This particular method is a difficult one. A further problem is lack of information concerning α_z, the accommodation coefficient. The value of α_z is not accurately known, but may possibly be assumed constant across the shock wave. For these reasons a non-dimensionalization and normalization process is employed as follows:

$$\dot{E}_{w_2} = \text{constant} = A I R_1 \alpha_1 \left\{ \sqrt{\frac{T_2}{T_1}} \left(\frac{\rho_2}{\rho_1}\right) \left(\frac{T_2}{T_1} f^\circ(s_2) - \frac{T_w}{T_1} g^\circ(s_2)\right) + \left(\frac{T_w}{T_1} - 1\right) g^\circ(0) \right\}$$

$$\dot{E}_{w_2} \equiv A I R_1 \alpha_1 D$$

where

$$s_2 = \frac{\sqrt{\frac{\gamma}{2}}\, M_s \left\{1 - \frac{\rho_1}{\rho_2}\right\}}{\sqrt{\frac{T_2}{T_1}}}$$

Therefore,

$$\frac{\dot{E}_w}{\dot{E}_{w_2}} = \frac{1}{D}\left\{\sqrt{\frac{T}{T_1}}\left(\frac{\rho}{\rho_1}\right)\left(\frac{T}{T_1} f^{\circ}(s) - \frac{T_w}{T_1} g^{\circ}(s)\right) + \left(\frac{T_w}{T_1} - 1\right) g^{\circ}(0)\right\} \quad (14)$$

where

$$D = \left\{\sqrt{\frac{T_2}{T_1}}\left(\frac{\rho_2}{\rho_1}\right)\left(\frac{T_2}{T_1} f^{\circ}(s_2) - \frac{T_w}{T_1} g^{\circ}(s_2) + \left(\frac{T_w}{T_1} - 1\right) g^{\circ}(0)\right\}\right.$$

This equation provides an easy means for comparison (see Data Reduction). It may be integrated to provide E_w.

C. Experimental Arrangement

a) Probe Construction

The probe was a bank of six very fine wires mounted in a standard plug designed for the GALCIT 17-inch shock tube. (See Ref. 4.) A drawing of the probe is included in Figure 1. The face of the plug was circular, approximately 40 mm in diameter and was flush with the end wall of the tube. Six glass to metal seals were mounted in the plug face. Milling dowel was soldered into the terminals of these seals, protruding 15/32" from the end wall. (Note that this distance allows the shock and some uniform flow to pass over the wire before the reflected shock returns (see Fig. 3).) Six cold wires were mounted across the dowels, equidistant from the end wall. The fine wires used were .00005" diameter (1/20 mil) platinum-rhodium ($Pt_{90}Rh_{10}$) Wollaston process wires (1/100 mil wires were studied but problems discussed in Appendix A precluded their use). The wire heating circuit was the usual circuit with ballast resistance to keep current constant. A detailed description of fine wire mounting is included in Appendix B.

b) Final Measurements

The GALCIT 17-inch shock tube has been described in detail in reference 4. A further discussion is presented in reference 5, while a modification of importance is reported in reference 6.

The probe described previously was mounted in the

stainless steel end wall of the shock tube. Various combinations of helium and nitrogen were employed in the driver section to obtain various Mach numbers (cf. Ref. 5). The gas in the driven section was argon, at initial pressures ranging from 25 μHg to 200 μHg. The 1/20 mil wire probes were electrically placed in series with a large resistor to assure constant current operation. A precision resistor, placed in series with the cold wire, was used to measure the current, by measuring voltage across it. All voltages were measured by digital voltmeters. A simple switching arrangement facilitated voltage, current, and resistance measurements.

The cold wire output was fed directly to a $\times 10^3$ amplifier and sent to the six "y" axes of three dual-beam Tektronix oscilloscopes. Three different scale settings were employed. The overall picture was viewed on oscilloscope 1 by using long-time scales (5 μsec/cm, see Fig. 3). Shorter time scales were employed on the other two oscilloscopes.

To assure an adequate measure of the linear wire response in region (2), the upper traces on the second two oscilloscopes were delayed by roughly 5 μsec to produce the lower traces (cf. Fig. 4). In the cases of short-time scales and thick shocks, the delayed upper trace was absolutely necessary to establish the reference. The data were recorded by photographing the oscilloscope response trace (Figs. 4 - 9).

A thin film heat transfer gauge was placed 24 mm upstream of the end wall of the shock tube to provide a triggering pulse as

the shock passed over it. This triggering device was located only 17/32" ahead of the cold wire probe (but 6" to one side). With this arrangement, the time between trigger and shock arrival was short enough (approximately 5 μsec) that no initial delay was required in the setup.

Shock Mach number was obtained by measuring the shock velocity between two film gauges 500 mm apart near the end wall.

D. Data Reduction

The oscillograms of the six final runs are shown in Figures 4 - 9. There is some inherent camera lens distortion on the oscillograms. This distortion reaches up to 10 per cent on the outer edges of the photographs. The 60 squares on the photographs were measured and each reading from an oscillogram was corrected for both horizontal and vertical distortion. The horizontal oscilloscope scales (time) were checked using a pulse generator to give a known time marker on the trace. The timing traces relative to the square grid were found to be 0 - 3 per cent in error. This was corrected. A calibrated voltage was supplied to the oscilloscopes and the vertical deflections of the traces were calibrated visually. This is believed to be sufficiently accurate, since in the normalization process the associated multiplicative error is divided out.

On the final six oscillograms which were used, abscissas and ordinates were read from a x 10 power optical comparator. The readings were accurate to within .001". The readings were made non-dimensional horizontally with the mean free path and shock speed, and with $dF_2/d\mathcal{Y}$ vertically. These data are included in Table I.

The data presented in the graphs and tables represent true response, without curve smoothing. These points, non-dimensionalized, are used in a numerical differentiation to obtain a curve for comparison with theory. If x_1, x_2, x_3, x_4, and x_5 are five successive equally spaced abscissas, placed in ascending order, the differentiation

formula employed (Ref. 7) was:

$$\frac{dy(x_3)}{dx} = \frac{1}{\Delta x}\left\{\frac{1}{12}y(x_1) - \frac{2}{3}y(x_2) + \frac{2}{3}y(x_4) - \frac{1}{12}y(x_5)\right\} \qquad (15)$$

Where:

$$\Delta x = x_2 - x_1 \; ; \; x_3 - x_2 \; ; \text{ etc.}$$

The x spacings of points from the data oscillograms were not equal but varied by only 1 - 3 per cent. A mean value of Δx was determined for each set of five points so that the calculations were as for equally spaced points.

All pertinent parameters such as wire resistance, temperatures, etc., are included in Table I for reference.

For comparison purposes, the data for the L-N-C and N-S theories were reduced and plotted. Available from both of these theories are the quantities u/u_1, ρ/ρ_1 and T/T_1 for substitution into equation (14). One may, using this equation, compare the differentiated oscillogram data with the L-N-C and N-S data.

To compare the two theories directly with the E_w versus t on the oscillograms, one must integrate equation (14):

$$\frac{E_w}{dE_{w_2}/d\tau} = \frac{1}{D}\int_0^t \left\{\sqrt{\frac{T}{T_1}}\left(\frac{\rho}{\rho_1}\right)\left(\frac{T}{T_1}f^\circ(s) - \frac{T_w}{T_1}g^\circ(s)\right) + \left(\frac{T_w}{T_1} - 1\right)g^\circ(0)\right\} d\tau \qquad (16)$$

With:

$$\tau = \frac{\pi \bar{V}_s t}{4 \Delta_1}$$

A time origin for the shock profile must be chosen arbitrarily. In the comparison of theory with experiment, time is a free parameter, which is compared by sliding the curves relative to each other to best exhibit the comparison.

TABLE I

Set No. 1 - Run 510

$T_1 = 298.26^{\circ}K$

$p_1 = 50\ \mu Hg$

$\rho_1 = 1.0747 \times 10^{-7}\ g/cm^3$

$\mu_1 = 22.536 \times 10^{-5}$ poises

$a_1 = 0.3216$ mm/μsec

$V_s = 1.598$ mm/μsec

$\Lambda_1 = 1.0543$ mm

$\pi V_s/4\Lambda_1 = 1.1897/\mu$sec

$T_w/T_1 = 1.2687$

$dE_2/d\mathcal{T} = 0.1916$ mv

$M_s = 4.967$

$I = 328.34\ \mu$amps

$R_w/R_1 = 1.1271$

$y_0 = .2705$ mv

$x_0 = 1.161$

TABLE I (CONTD.)

$\frac{\pi V_s (x - x_0)}{4 \Lambda_1}$	$\frac{E - y_0}{dE_2/d\vartheta}$	$\dot{E}/\dot{E}_2$	$\frac{\pi V_s (x - x_0)}{4 \Lambda_1}$	$\frac{E - y_0}{dE_2/d\vartheta}$	$\dot{E}/\dot{E}_2$
--	0	0	4.645	1.388	.8211
--	0	0	4.876	1.557	.7640
--	0	0	5.112	1.746	.8259
0	0	.0295	5.338	1.933	.7965
.226	.0016	.0317	5.572	2.119	.8996
.460	.0042	.0493	5.806	2.338	.9105
.692	.0251	.111	6.033	2.529	.7895
.919	.0517	.104	6.266	2.705	.7789
1.161	.0720	.0805	6.496	2.888	.8013
1.393	.0898	.0728	6.724	3.084	.9851
1.640	.1065	.0636	6.967	3.333	1.0588
1.850	.1232	.1120	7.195	3.550	.8354
2.082	.1634	.2510	7.418	3.723	.8364
2.322	.2333	.2670	7.648	3.935	.8022
2.549	.2850	.2310	7.882	4.105	1.005
2.785	.3481	.3340	8.128	4.391	1.0794
3.013	.4379	.4193	8.36	4.591	.8281
3.242	.5350	.3440	8.60	4.793	.9276
3.484	.6049	.3930	8.831	5.014	.9351
3.713	.7255	.5660	9.064	5.220	.7969
3.944	.8648	.6960	9.289	5.447	.9794
4.170	1.038	.6750	9.523	5.665	1.000
4.405	1.181	.7601	9.758	5.901	1.000

TABLE I (CONTD.)

Set No. 2 - Run 503

$T_1 = 299.26^{\circ}$ K

$p_1 = 100\,\mu$ Hg

$\rho_1 = 2.1422 \times 10^{-7}$ gm/cm^3

$\mu_1 = 22.6 \times 10^{-5}$ poises

$a_1 = 0.3223$ mm/μsec

$V_s = 1.76$ mm/μsec

$\Lambda_1 = .5275$ mm

$\pi V_s/4\Lambda_1 = 2.6205/\mu$sec

$T_w/T_1 = 1.2889$

$dE_2/d\Upsilon = .2204$ mv

$M_s = 5.462$

$I = 354.1\,\mu$ amps

$R_w/R_1 = 1.1371$

$y_0 = 0.02564$ mv

$x_0 = 1.2814$

TABLE I (CONTD.)

$\frac{\pi V_s(x - x_0)}{4\Lambda_1}$	$\frac{E - y_0}{dE_2/d\vartheta}$	$\dot{E}/\dot{E}_2$	$\frac{\pi V_s(x - x_0)}{4\Lambda_1}$	$\frac{E - y_0}{dE_2/d\vartheta}$	$\dot{E}/\dot{E}_2$
--	0	0	5.379	1.242	.7545
--	0	0	5.631	1.441	.7381
0	0	.0897	5.888	1.615	.6831
.250	.0434	.1586	6.140	1.800	.7571
.523	.0725	.0887	6.408	1.999	.7154
.768	.0899	.0562	6.663	2.169	.6787
1.016	.1015	.0206	6.917	2.363	.8943
1.282	.1018	0	7.169	2.614	.9492
1.546	.1042	.0494	7.425	2.825	.5724
1.785	.1244	.0554	7.689	2.938	.6628
2.041	.1303	.0287	7.943	3.185	1.0255
2.296	.1418	.0424	8.199	3.444	1.0272
2.563	.1563	.1272	8.457	3.698	.8862
2.812	.2024	.1616	8.703	3.912	.9578
3.071	.2371	.1703	8.970	4.188	.9277
3.324	.2893	.1897	9.231	4.397	.9163
3.573	.3356	.2110	9.500	4.672	1.000
3.845	.4023	.2927	9.746	4.910	.9986
4.101	.4885	.3961	10.005	5.182	.9985
4.354	.6073	.4905	10,252	5.414	.8916
4.615	.7375	.5582	10.520	5.645	.9324
4.865	.8936	.6369	10.770	5.886	1.000
5.126	1.061	.6836	11.021	6.106	1.000

TABLE I (CONTD.)

Set No. 3 - Run 504

$T_1 = 300.26^{\circ}K$

$p_1 = 200\ \mu$ Hg

$\rho_1 = 4.2701 \times 10^{-7}$ gm/cm^3

$\mu_1 = 22.664 \times 10^{-5}$ poises

$a_1 = 0.323$ mm/μsec

$V_s = 1.661$ mm/μsec

$\Lambda_1 = .2657$ mm

$\pi V_s/4\Lambda_1 = 4.9104/\mu$sec

$T_w/T_1 = 1.2669$

$dE_Z/d\tau = .1755$ mv

$M_s = 5.143$

$I = 357.5\ \mu$amps

$R_w/R_1 = 1.1123$

$y_0 = 0.3078$ mv

$x_0 = 9.605$

TABLE I (CONTD.)

$\frac{\pi V_s(x - x_0)}{4\Lambda_1}$	$\frac{E - y_0}{dE_2/d\tau}$	$\dot{E}/\dot{E}_2$	$\frac{\pi V_s(x - x_0)}{4\Lambda_1}$	$\frac{E - y_0}{dE_2/d\tau}$	$\dot{E}/\dot{E}_2$
0	0	--	10.539	6.167	.9192
.468	.0051	--	11.042	6.594	.9254
.951	.0268	.1004	11.512	7.064	.9790
1.419	.0997	.1670	12.006	7.535	.9956
1.893	.1869	.2231	12.470	8.022	1.000
2.401	.3174	.3010	12.956	8.543	1.000
2.883	.4746	.3411			
3.358	.6490	.3918			
3.834	.8519	.4575			
4.316	1.084	.4852			
4.802	1.326	.5599			
5.272	1.639	.7997			
5.751	2.067	.8620			
6.227	2.443	.7773			
6.709	2.828	.8149			
7.203	3.226	.8193			
7.680	3.614	.7998			
8.154	3.998	.8158			
8.628	4.385	.8798			
9.098	4.837	.8931			
9.604	5.254	.9098			
10.077	5.711	.9523			

TABLE I (CONTD.)

Set No. 4 - Run 511

$T_1 = 297.66^{\circ}K$

$p_1 = 25\ \mu Hg$

$\rho_1 = 0.5385 \times 10^{-7}\ gm/cm^3$

$\mu_1 = 22.498 \times 10^{-5}$ poises

$a_1 = 0.3214\ mm/\mu sec$

$V_s = 2.273\ mm/\mu sec$

$\Lambda_1 = 2.1019\ mm$

$\pi V_s/4\Lambda_1 = 0.8493/\mu sec$

$T_w/T_1 = 1.2563$

$dE_2/d\Upsilon = 0.3853\ mv$

$M_s = 7.071$

$I = 337.19\ \mu amps$

$R_w/R_1 = 1.121$

$y_0 = 0.2564\ mv$

$x_0 = 0.1658$

TABLE I (CONTD.)

$\frac{\pi V_s (x - x_0)}{4\Lambda_1}$	$\frac{E - y_0}{dE_2/d\tau}$	$\dot{E}/\dot{E}_2$	$\frac{\pi V_s (x - x_0)}{4\Lambda_1}$	$\frac{E - y_0}{dE_2/d\tau}$	$\dot{E}/\dot{E}_2$
0	0	--	3.8084	1.5674	.8850
.1570	.0701	--	3.9788	1.7379	.8962
.3271	.0849	.0792	4.1419	1.8853	.8373
.4929	.1033	.0652	4.1419	2.0192	.8652
.6631	.1082	.0568	4.4682	2.1690	.8816
.8289	.1256	.1290	4.6344	2.3135	.9319
.9904	.1505	.1836	4.8077	2.4788	.9491
1.1594	.1838	.1721	4.9697	2.6306	.9899
1.3251	.2087	.1929	5.1349	2.8082	1.0936
1.4902	.2484	.2395	5.2970	2.9810	1.000
1.6478	.2870	.2828	5.4600	3.1419	.9531
1.8143	.3403	.3071	5.6366	3.3008	.9741
1.9796	.3883	.3236	5.7990	3.4671	.9929
2.1470	.4547	.5036	5.9646	3.6319	1.000
2.3210	.5494	.5180	6.1301	3.7949	1.000
2.4776	.6273	.5433			
2.6480	.7301	.6037			
2.8068	.8246	.6245			
2.9762	.9406	.6868			
3.1499	1.0516	.6943			
3.3134	1.1767	.0857			
3.4781	1.3159	.8262			
3.6407	1.4482	.8194			

TABLE I (CONTD.)

Set No. 5 - Run 509

$T_1 = 298.66^{\circ}K$

$p_1 = 50\ \mu Hg$

$\rho_1 = 1.0733 \times 10^{-7}\ gm/cm^3$

$\mu_1 = 22.562 \times 10^{-5}$ poises

$a_1 = 0.3221\ mm/\mu sec$

$V_s = 2.392\ mm/\mu sec$

$\Lambda_1 = 1.0553\ mm$

$\pi V_s/4\Lambda_1 = 1.7802/\mu sec$

$T_w/T_1 = 1.3673$

$dE_2/d\Upsilon = 0.4461\ mv$

$M_s = 7.427$

$I = 350.19\ \mu amps$

$R_w/R_1 = 1.174$

$y_0 = 0.0358\ mv$

$x_0 = 3.4750$

TABLE I (CONTD.)

$\frac{\pi V_s (x - x_0)}{4 \Lambda_1}$	$\frac{E - y_0}{dE_2/d\tau}$	$\dot{E}/\dot{E}_2$	$\frac{\pi V_s (x - x_0)}{4 \Lambda_1}$	$\frac{E - y_0}{dE_2/d\tau}$	$\dot{E}/\dot{E}_2$
0	0	0	7.9825	3.9181	.9690
.3489	0	.0221	8.3357	4.2433	.7296
.6932	.0143	.0366	8.6873	4.4372	.7070
1.0423	.0229	.0228	9.0302	4.7524	.9624
1.3775	.0316	.0209	9.3772	5.0763	.9970
1.7374	.0430	.0766	9.7243	5.4229	1.000
2.0794	.0888	.1741	10.0648	5.7582	.9910
2.4210	.1632	.2633	10.4248	6.1048	1.000
2.7737	.2634	.2694	10.776	6.4515	1.000
3.1108	.3548	.328			
3.4749	.4952	.4322			
3.8114	.6487	.459			
4.1610	.8175	.535			
4.5019	1.0177	.6178			
4.8471	1.2436	.7245			
5.2124	1.5095	.7919			
5.5565	1.7758	.7354			
5.8986	2.0186	.7630			
6.2406	2.2983	.8140			
6.5917	2.5926	1.1080			
6.9499	3.0295	1.0910			
7.2940	3.3164	.7999			
7.6361	3.6045	.8789			

TABLE I (CONTD.)

Set No. 6 - Run 506

$T_1 = 299.36^{\circ}K$

$p_1 = 100\ \mu Hg$

$\rho_1 = 2.1415 \times 10^{-7}\ gm/cm^3$

$\mu_1 = 22.607 \times 10^{-5}$ poises

$a_1 = 0.3225\ mm/\mu sec$

$V_s = 2.4271\ mm/\mu sec$

$\Lambda_1 = 0.5293\ mm$

$\pi V_s/4\Lambda_1 = 3.601/\mu sec$

$T_w/T_1 = 1.305$

$dE_2/d\tau = 0.3903\ mv$

$M_s = 7.526$

$I = 347.5\ \mu amps$

$R_w/R_1 = 1.1448$

$y_0 = 0.8241\ mv$

$x_0 = 2.8225$

TABLE I (CONTD.)

$\frac{\pi V_s (x - x_0)}{4\Lambda_1}$	$\frac{E - y_0}{dE_2/d\tau}$	$\dot{E}/\dot{E}_2$	$\frac{\pi V_s (x - x_0)}{4\Lambda_1}$	$\frac{E - y_0}{dE_2/d\tau}$	$\dot{E}/\dot{E}_2$
0	0	0	8.0961	3.6907	.8238
.3543	.0133	0	8.4450	3.9907	.8844
.6993	.0364	.0576	8.7961	4.3102	.8956
1.0417	.0566	.0921	9.1519	4.6231	.9365
1.3928	.1058	.1842	9.5037	4.9687	.9370
1.7558	.1814	.2189	9.8577	5.2928	1.0956
2.1004	.2601	.2509	10.2027	5.7163	1.000
2.4602	.3587	.2938	10.5527	5.9833	.7960
2.7976	.4671	.3561	10.893	6.3089	.9597
3.1552	.6049	.3862	11.2646	6.6627	1.000
3.5016	.7328	.3619	11.6251	7.0340	1.000
3.8527	.8706	.4495			
4.2211	1.0476	.4874			
4.5689	1.2185	.5519			
4.9233	1.4376	.6127			
5.2707	1.6436	.6046			
5.6276	1.8657	.6159			
5.9819	2.0781	.6391			
6.3266	2.3177	.7097			
6.6708	2.5721	.7527			
7.0241	2.8432	.7948			
7.3773	3.1340	.7883			
7.7428	3.4045	.7820			

E. Results

The experiment required development of a probe with wires smaller than those employed by Christiansen (Ref. 2). All pertinent wire equations, however, were taken from his work. In going to smaller wires, the instrument became very fragile (the fine wires were broken or melted during each shock tube firing).

Some preliminary shock structure measurements were made; the resulting oscillograms are presented in Figures 4 - 9. The non-dimensionalized oscillogram readings are shown in Figures 10 - 15. Navier-Stokes and Liepmann-Narasimha-Chahine data have been plotted along with wire response in two ways: the oscillogram values have been compared with the integrated N-S and L-N-C data (Figs. 10 - 15); and, the differentiated response curves have been compared with N-S and L-N-C through the normalized Stalder theory (Figs. 16, 17).

Three runs were made at $M_s = 5$ and three at $M_s = 7.5$ using different initial pressures (both Mach numbers are $\pm 6\frac{1}{2}$ per cent). Initial pressures were changed by multiples of two to best exhibit thickness dependence upon mean free path. Apparent thicknesses were roughly as follows:

	$M_s \doteq 5$	$M_s \doteq 7.5$
$p_1 =$ 25 μHg	--	20.2 mm
50 μHg	10.4 mm	13 mm
100 μHg	4.9 mm	7.3 mm
200 μHg	3.1 mm	--

In presenting the differentiated curves, the results of all three shots for both Mach numbers were superimposed after non-dimensionalization and normalization (Figs. 16, 17). These figures show that the curves superimpose quite well and tend to define a shock structure. The numerical differentiation gives scatter where the curve changes its slope from zero to a finite value and from a finite value to zero. Some electrical noise was observed which caused scatter in the differentiated curve (see especially Fig. 4).

Ionization effects are clearly seen in Figure 18. The primary ionization effect is in region (5) behind the reflecting shock wave.

III. CONCLUSIONS

An attempt has been made to measure shock wave structure in terms of heat transfer rate to a fine cold wire over which the wave passes. Christiansen (Ref. 2) points out that sufficient wire sensitivity is very difficult to obtain. This experiment employed several wires in series in an attempt to overcome sensitivity difficulties. The difference between N-S and the L-N-C theories at $M_s = 5$ is shown in Figure 10. The small difference between the two clearly indicates the need for increased sensitivity. As is evident from Figure 4, a further improvement in signal-noise ratio is necessary. Further increasing the wire length can provide signal improvement to any degree desired.

The systematic discrepancy between measured and theoretical heat-transfer profiles (Fig. 10 and Fig. 16) indicates that a possible cold wire problem may exist. The measured data give a larger apparent shock thickness than theory. One explanation for the discrepancy may be that more of a strain gauge effect exists than was estimated (cf. p. 37). Another possibility might be the effect proposed by Clarke (Ref. 15) that a lag is introduced by a surface energy-accommodation effect. Some ionization in region (2) may also produce a false apparent thickening of the shock. These effects must be investigated and the region (2) reference must be established beyond a doubt by some calibration procedure before a shock profile can be absolutely established.

REFERENCES

1. Stalder, Jackson R.; Goodwin, Glen; and Creager, Marcus O.: A Comparison of Theory and Experiment for High Speed Free-molecule Flow. NACA TN 2244, 1950.

2. Christiansen, Walter H.: Development and Calibration of a Cold Wire Probe for Use in Shock Tubes. Ph. D. Thesis, Calif. Inst. of Technology, 1961.

3. Liepmann, Hans W.; Narasimha, R.; and Chahine, M. T.: Structure of a Plane Shock Layer. Phys. of Fluids, 5, 1313-1324, 1962.

4. Liepmann, H. W.; Roshko, A.; Coles, D.; and Sturtevant, B.: A 17-Inch Diameter Shock Tube for Studies in Rarefied Gasdynamics. Rev. Scientific Instruments, 33, No. 6, 625-631, June 1962.

5. Johnson, Douglas S.: Design and Application of Piezoceramic Transducers to Transient Pressure Measurements, II. Some Measurements of Curvature and Thickness of Reflecting Normal Shocks at Low Initial Pressures. Thesis, Calif. Inst. of Technology, 1962.

6. Slachmuylders, Erik: Measurements of the Acceleration of Reflected Shock Waves by Means of a New Heat Transfer Gauge. Thesis, Calif. Inst. of Technology, 1963.

7. Hartree, D. R.: Numerical Analysis. The Clarendon Press, Oxford, 1952.

8. Cole, J.; and Roshko, A.: Heat Transfer from Wires at Reynolds Numbers in the Oseen Range. Proc. 1954 Heat Transfer and Fluid Mechanics Institute.

9. Sherman, F. S.: A Low-density Wind-tunnel Study of Shock-wave Structure and Relaxation Phenomena in Gases. NACA TN 3298, 1955.

10. Mueller, James N.: Equations, Tables, and Figures for Use in the Analysis of Helium Flow at Supersonic and Hypersonic Speeds. NACA TN 4063, 1957.

11. Keyes, Frederick G.: The Heat Conductivity, Viscosity, Specific Heat and Prandtl Numbers for Thirteen Gases. Project Squid T. R. 37, 1952.

12. Vines, Raymond F.: The Platinum Metals and Their Alloys. International Nickel Company, New York, 1941.

13. Hodgman, Charles D. (editor): Handbook of Chemistry and Physics. Chemical Rubber Company, Cleveland, Ohio, 1949.

14. Tables of Thermal Properties of Gases. N.B.S. Circular 564, November 1955.

15. Clarke, John F.: Temperature-time Histories at the Interface Between a Gas and a Solid. College of Aeronautics, Cranfield, England, 1961.

APPENDIX A

DISCUSSION OF VERY FINE WIRES

One of the main aims of this experiment was to investigate the feasibility of using very fine cold wires for times short enough to study shock structure. .00001" diameter (1/100 mil) and .00005" diameter (1/20 mil) platinum-rhodium wires were used. Some of the characteristics of cold wires, described in detail by Christiansen (Ref. 2), are summarized below.

A body in a flowing gas is characterized by a "recovery" temperature. This is the temperature that an unheated wire would reach if it were allowed to come to thermal equilibrium with the flow. A common hot wire is one which operates at a higher temperature than the recovery value and, therefore, loses heat to the flow. A cold wire works in the opposite manner, having lower initial temperature than the recovery temperature. It therefore gains heat from the flow. Very high recovery temperatures are characteristic of the flow behind strong shock waves. This, in conjunction with relatively low wire melting temperature, precludes the use of hot wires as opposed to cold wires.

a. Thermal Response

Christiansen (Ref. 2) provides an experimental curve of

$$\frac{\Delta}{d} \text{ versus } \frac{I^2 \sigma}{d^2 \kappa (T_w - T_1)}$$

For $(T_w - T_1)$ to be no more than $1^{\circ}C$, currents of only about 20 μamps for 1/100 mil wires can be used for initial pressures from 20 - 500 μHg. Simple calculations show, however, that it is necessary to increase the current to about 70 μamps to allow a 1/100 mil wire of about 1/16" length to operate above the noise level of the electronic system used. (Effective input noise level was about 30 μvolts.) Currents of up to 350 μamps are used for 1/20 mil wires.

b. Characteristic Times

The time for a wire to reach equilibrium temperature when a change in its environment occurs, i.e., the lag time constant, is of the order (Ref. 2),

$$t \sim \frac{d^2 \rho_w c_w}{4 Nu\, k} \tag{18}$$

For a 1/100 mil wire at 100 μHg pressure, this "lag" is of the order of a millisecond. It is, of course, longer for 1/20 mil wires.

Another characteristic time must also be taken into account. The time required for a temperature applied to the surface to penetrate to the wire's center is proportional to (Ref. 2)

$$t \sim \frac{d^2 \rho_w c_w}{k_w}$$

For a 1/100 mil wire, this time is of the order of .0006 μsec

and is approximately .01 μsec for a 1/20 mil wire. One assumes, therefore, that the temperature of the wires in this experiment are uniform across the cross-section at all times.

c. Miscellaneous Experiments

In the Stalder equation (Eq. (10)), the quantity T_w/T_1 is needed. Equation (1) shows the relation between T_w/T_1, R_w/R_1, and α_1. R_w and R_1 are measured directly and T_w/T_1 is obtained once α_1 is known. A simple oven experiment was conducted to determine α_1. Wires were placed in an oven and wire resistance for various temperatures was measured, with the following results (see Fig. 19):

Diameter	No. of Wires	Mean α_1
.00001"	5	.00157 Ω/°K
.00005"	15	.001586 Ω/°K

At low pressures (50 - 100 μHg), 1/100 mil wires burn out at currents in the neighborhood of 140 μamps. 1/20 mil wires withstand as much as 700 μamps. At atmospheric pressure, 1/100 mil wires withstand 3 milliamps and 1/20 mil withstand 10 milliamps.

Wire resistance versus pressure for values of constant current are shown in Figure 20, showing the effect of molecular density on heat transfer.

A phenomenon was observed when current versus resistance was measured at low pressure. The behavior of the 1/100 mil

wires is linear to a value of current near 70 μ amps (Fig. 21). Near this current, the resistance increases appreciably for a small current increase. It was found that a permanent hysteresis effect occurred, producing approximately a 60 per cent increase in zero current resistance. This effect, once it is allowed to run its course in changing resistance, produces a stable wire state where no further hysteresis effect occurs (Fig. 22). This effect is referred to as "annealing".

It seemed that with this effect one might increase the resistance of the wire and so improve output, but it was found that in this process α_1 had been halved, to .000785 $\Omega/^{o}K$ so the gain was more than offset. Shock tube preliminary runs showed that, at a certain point in the response of a 1/100 mil wire to a shock, the rate of increase of voltage of an "un-annealed" wire suffered a sudden decrease of slope at some point (Fig. 23). This reduction is consistent with the phenomena observed as it indicates a drop in α_1. The best explanation for this oddity seems to be that remnants of silver coating remain on the etched Wollaston wire and, when the wire is heated at low pressure, these particles are adsorbed into the wire. This causes a resistance increase due to diameter reduction and a resistivity coefficient drop due to silver interspersion within the crystal lattice. At room pressure oxidation apparently occurs at high wire temperatures, disallowing the "annealing" effect. Further work in this area has not been pursued.

d. Use of 1/100 and 1/20 Mil Wires in Shock Measurements

In preliminary shock tube runs, low initial pressure shots provided responses from the 1/100 mil wire which appeared reasonable. Three criteria were established for responses to be considered acceptable: First, one should be able to show that the response of the wire for the times involved should be linear in the uniform flow in region (2); second, one should be able to demonstrate that shock thickness is directly proportional to mean free path; third, one should demonstrate that no appreciable shock structure is present at high initial pressures, i.e., one should observe a ramp function on sweep speeds of the order 1 μsec/cm. The 1/100 mil wire failed all three tests. (cf. Fig. 24.)

Basic calculations reveal that strain, due to dynamic pressure, produces a voltage response similar to that of a strain gauge. More than 10 per cent of the resistance change for a 1/100 mil wire at 100 μHg pressure and $M_s = 5$ is due to strain. For a 1/20 mil wire in the same situation, the effect is less than 1 per cent.

In the normal process of hot and cold wire work, wires of large diameters are heated at atmospheric pressure to glowing before usage. A zero current resistance change of 2 - 4 per cent is experienced. This is done to burn off impurities. This practice was attempted on 1/100 mil wires but proved difficult because of a need for extremely sensitive current changes during the process. 1/20 mil wires are glowed at about 9.8 milliamps successfully.

1/20 mil wires met the three established criteria and,

because it is possible to easily glow the wires in atmospheric conditions, it was decided to use this wire exclusively rather than attempt strain compensation for the 1/100 mil wire.

The 1/20 mil six-wire probe attained approximately the same sensitivity as the single 1/100 mil probe by maintaining approximately the same ℓ/d ratio and the same $R_w I$ product (note that 1/20 mil "un-annealed" wires have nearly double the a_1 of "annealed" 1/100 mil wires).

APPENDIX B

FINE WIRE MOUNTING

A simple method of fine wire mounting was employed. Approximately 1/16" of the tip of the silver coated Wollaston wire was dipped into paste solder flux (any grease will suffice). The wires were then etched in a nitric acid solution; the function of the grease coat was to keep the end of the wire from etching, in order to provide a weight which kept the wire stretched vertically, made it easy to keep track of, and prevented air currents from blowing it around. The bare wire was then dipped into ether to clean it. Once cleaned, the wire was soldered to one of the dowels which had been tinned. The probe was rotated until the fine wire contacted the second dowel and was soldered into place. Wires as small as 1/200 mil have been mounted in this manner.

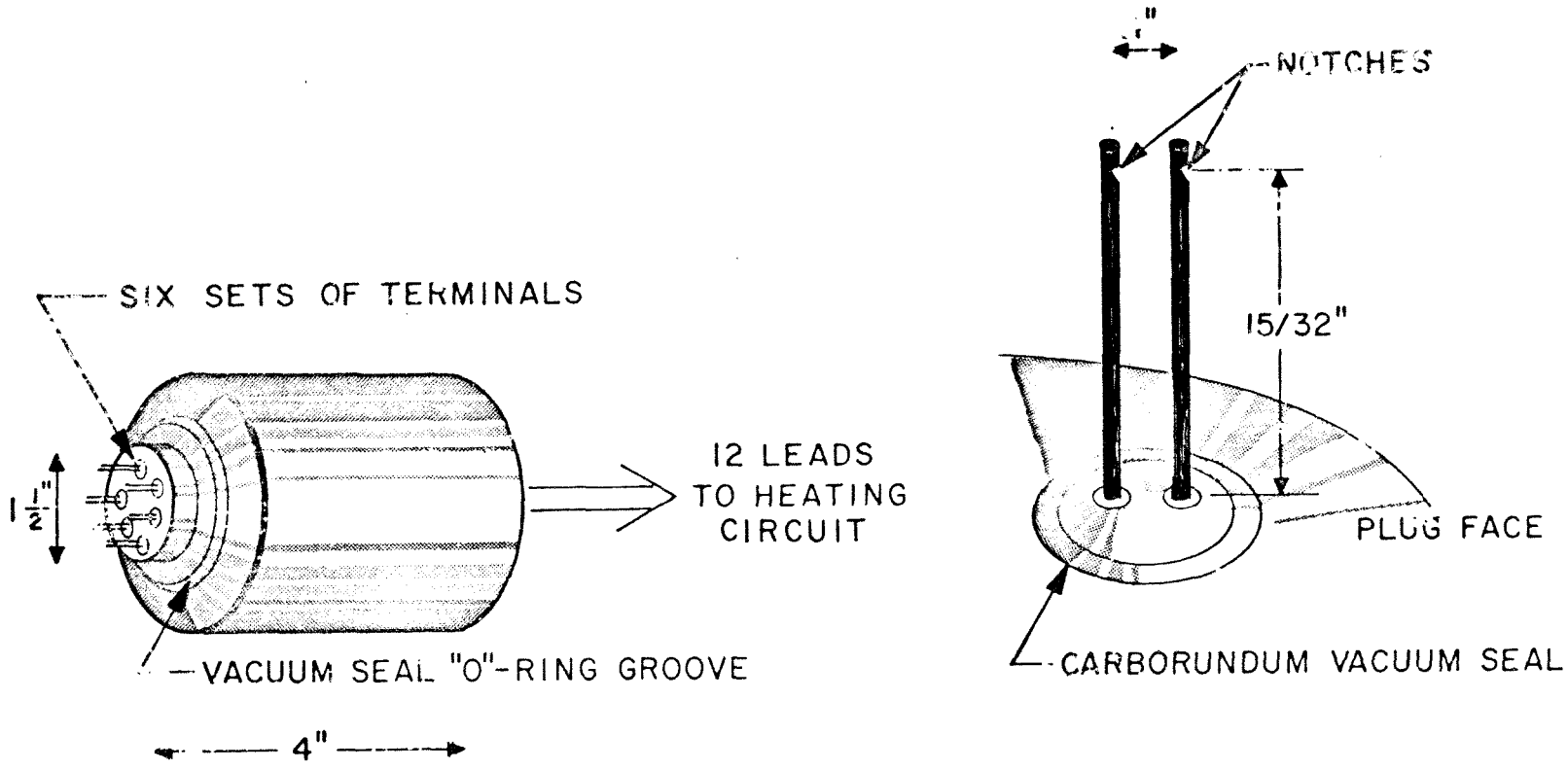

Fig. 1. Probe construction

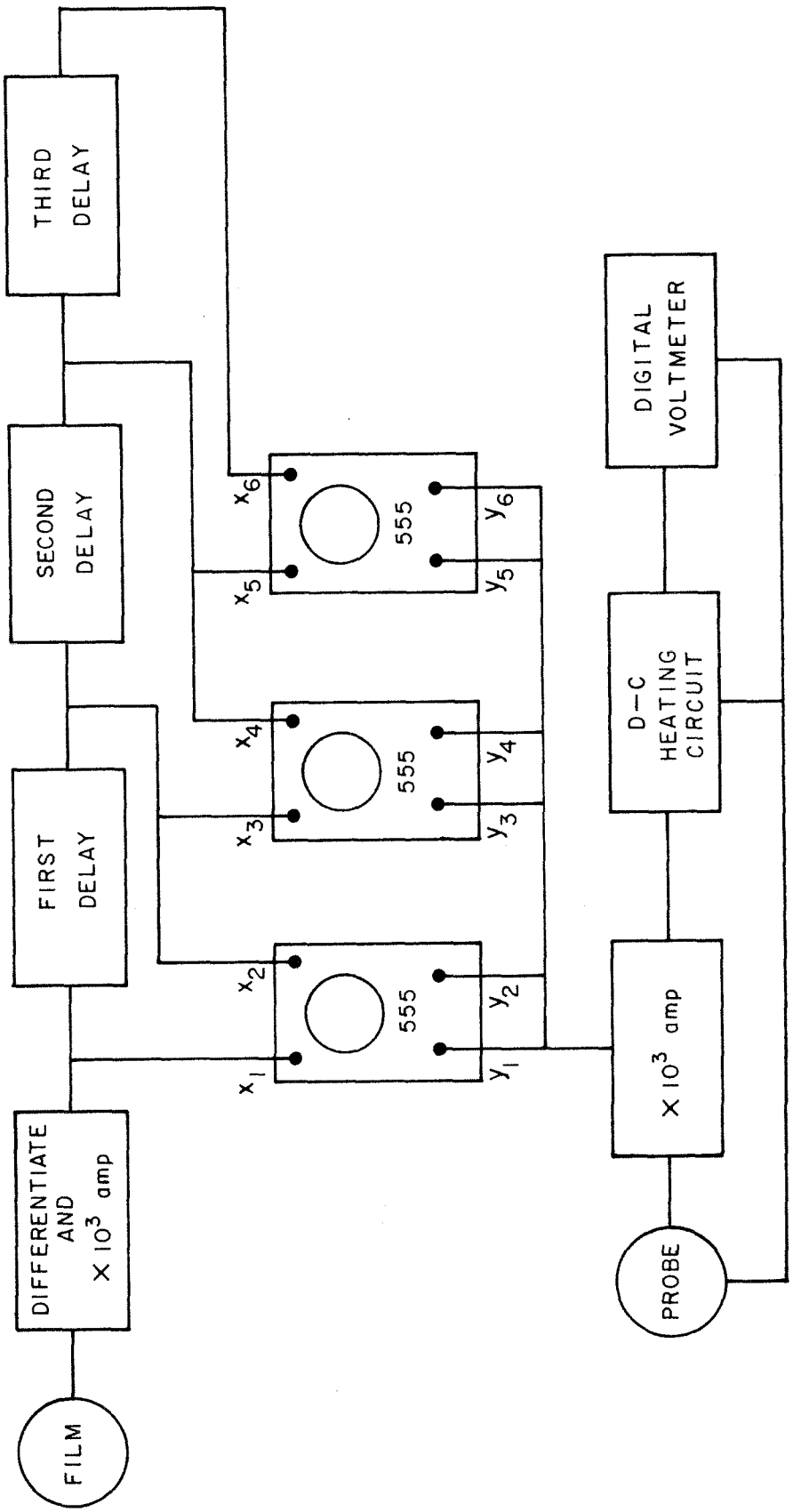

Fig. 2. Block Diagram of Experiment

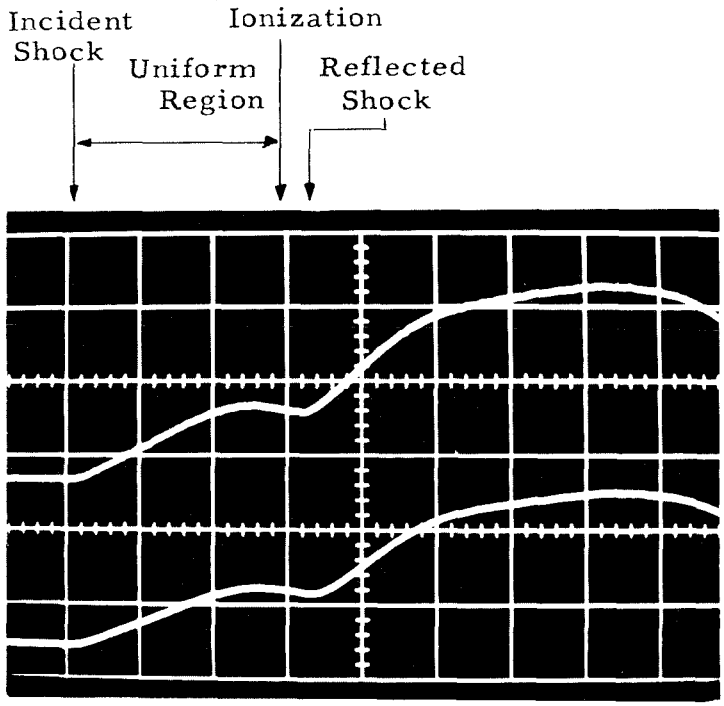

Upper: 1 mv/cm, 5 μsec/cm

Lower: 5 mv/cm, 5 μsec/cm

$p_1 = 100$ μHg $\qquad$ $M_s \doteq 7.5$

Fig. 3. Long Time Scale Shock Tube Run

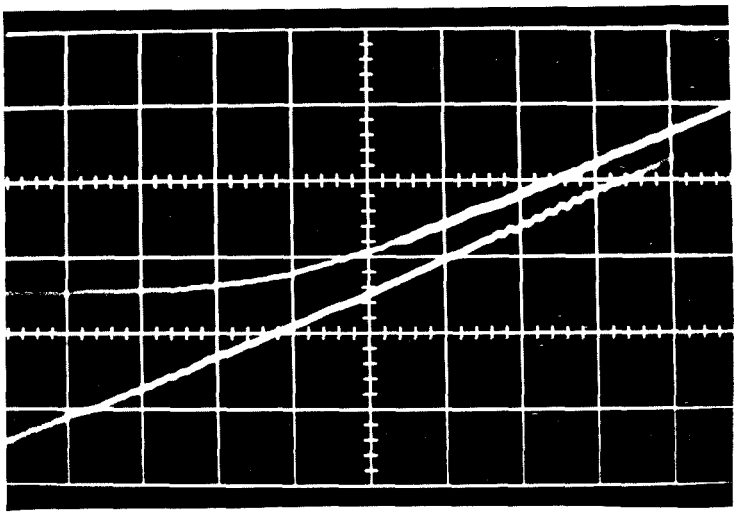

Upper: .5 mv/cm, 1 μsec/cm

Lower: Top Delayed 5 μsec

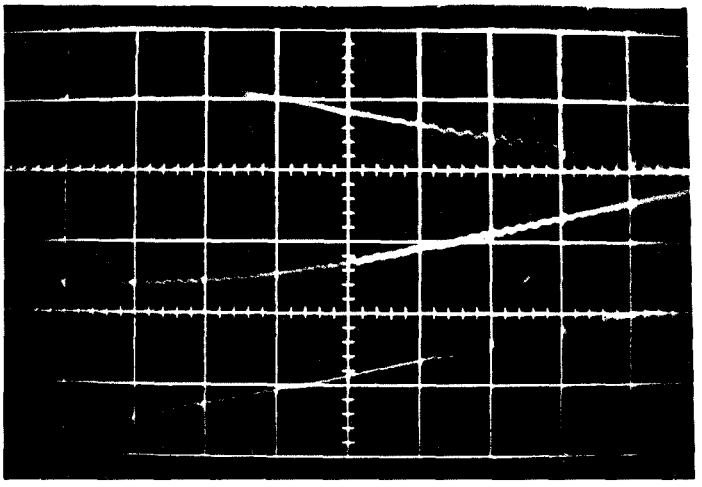

Upper: 1 mv/cm, 1 μsec/cm

Lower: Top Delayed 5 μsec

$p_1 = 50$ μHg $\qquad M_s \doteq 5$

Fig. 4. Cold Wire Oscillogram

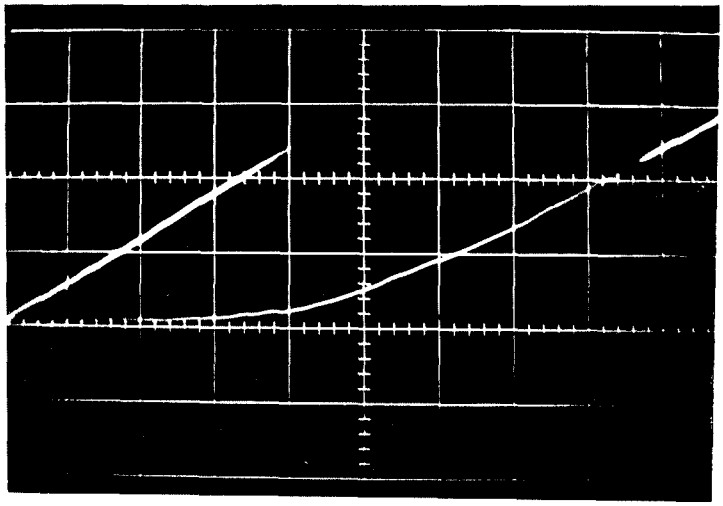

Upper: .5 mv/cm, .5 μsec/cm

Lower: Top Delayed 5 μsec

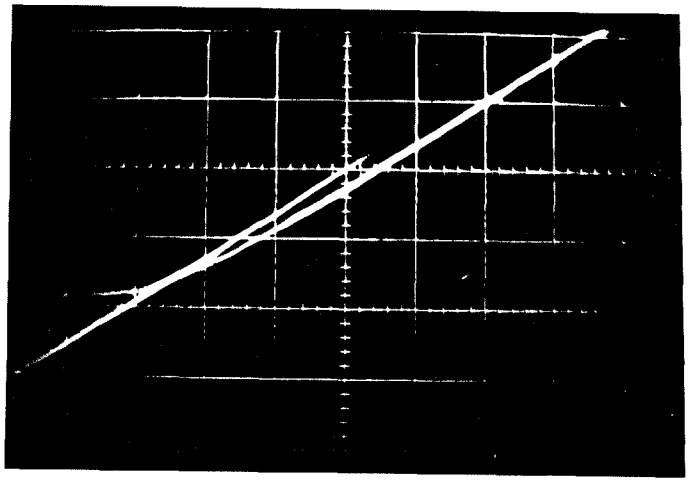

Upper: 1 mv/cm, 1 μsec/cm

Lower: Top Delayed 5 μsec

p_1 = 100 μHg $M_s \doteq 5$

Fig. 5. Cold Wire Oscillogram

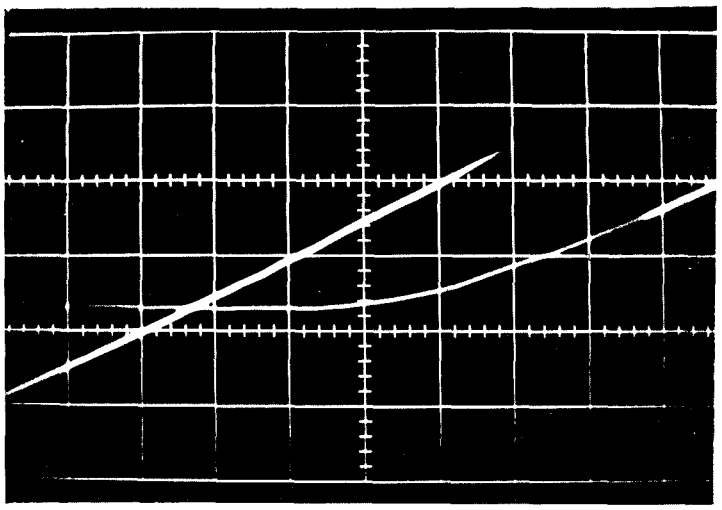

Upper: 1 mv/cm, .5 μsec/cm

Lower: Top Delayed 5 μsec

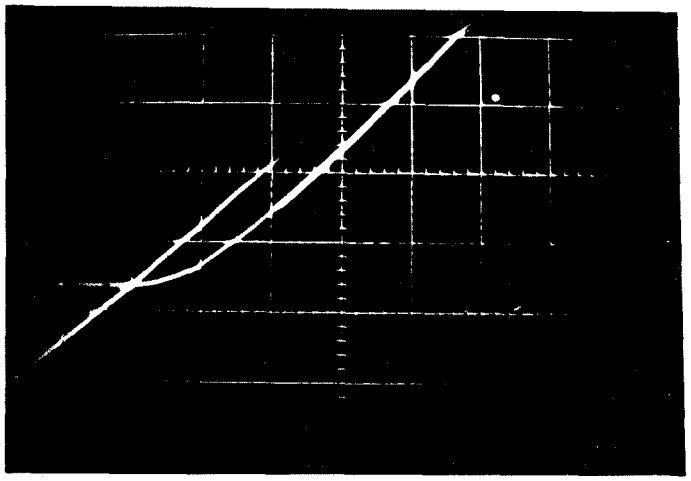

Upper: 1 mv/cm, 1 μsec/cm

Lower: Top Delayed 5 μsec

p_1 = 200 μHg $M_s \doteq 5$

Fig. 6. Cold Wire Oscillogram

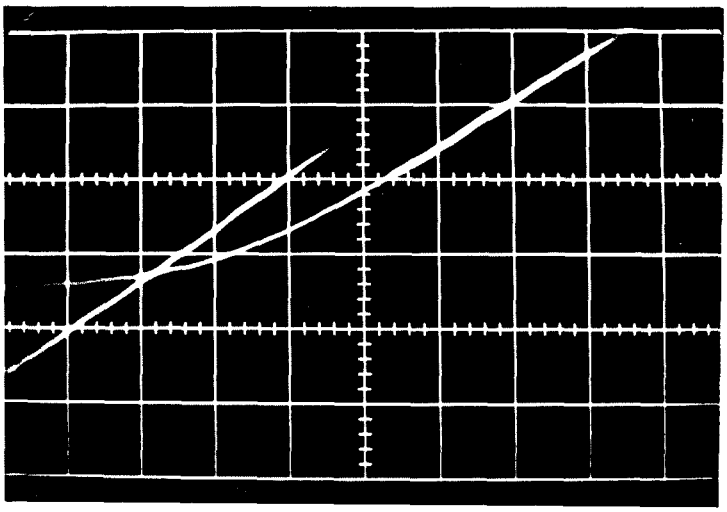

Upper: .5 mv/cm, 1 μsec/cm

Lower: Top Delayed 5 μsec

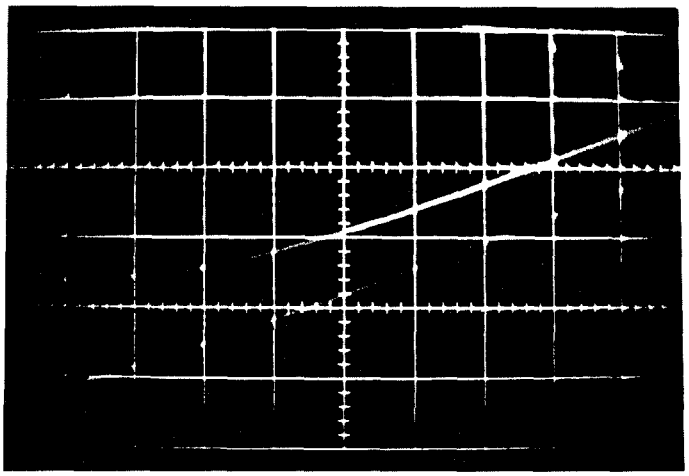

Upper: 1 mv/cm, 1 μsec/cm

Lower: Top Delayed 5 μsec

$p_1 = 25$ μHg $\qquad M_s \doteq 7.5$

Fig. 7. Cold Wire Oscillogram

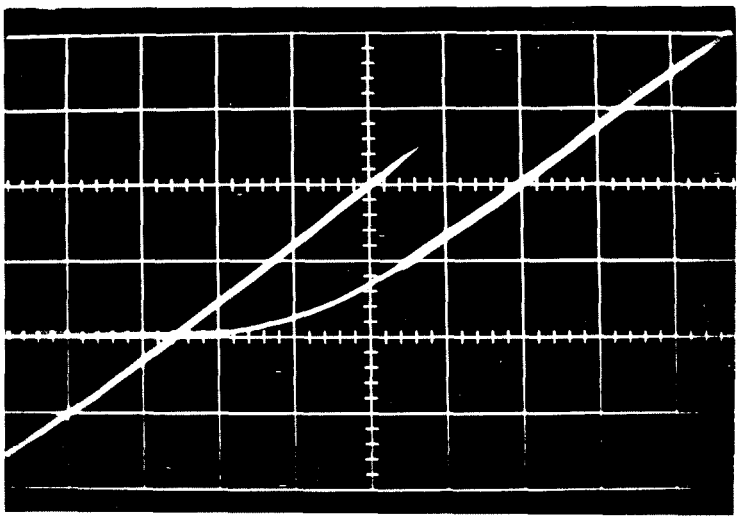

Upper: 1 mv/cm, 1 μsec/cm

Lower: Top Delayed 5 μsec

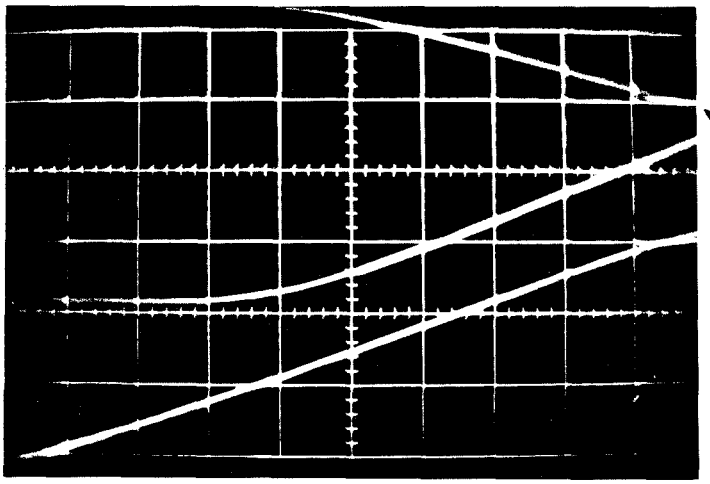

Upper: 2 mv/cm, 1 μsec/cm

Lower: Top Delayed 5 μsec

p_1 = 50 μHg $M_s \doteq 7.5$

Fig. 8. Cold Wire Oscillogram

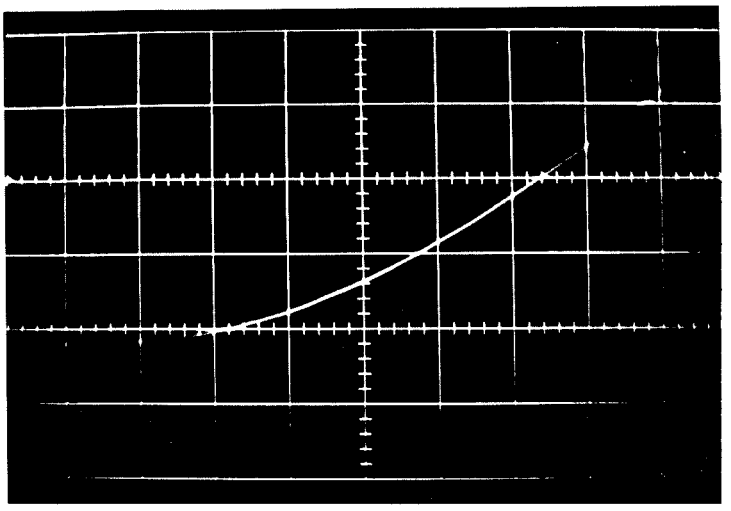

Upper: 1 mv/cm, .5 μ sec/cm

Lower: Top Delayed 5 μ sec

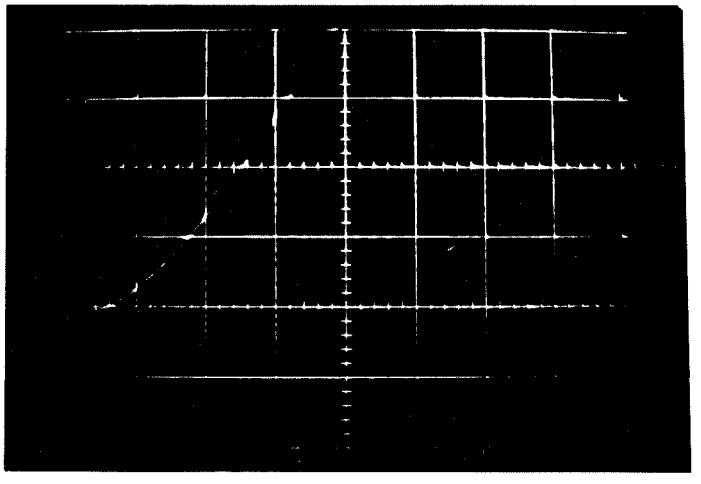

Upper: 1 mv/cm, 1 μ sec/cm

Lower: Top Delayed 5 μ sec

p_1 = 100 μHg $M_s \doteq 7.5$

Fig. 9. Cold Wire Oscillogram

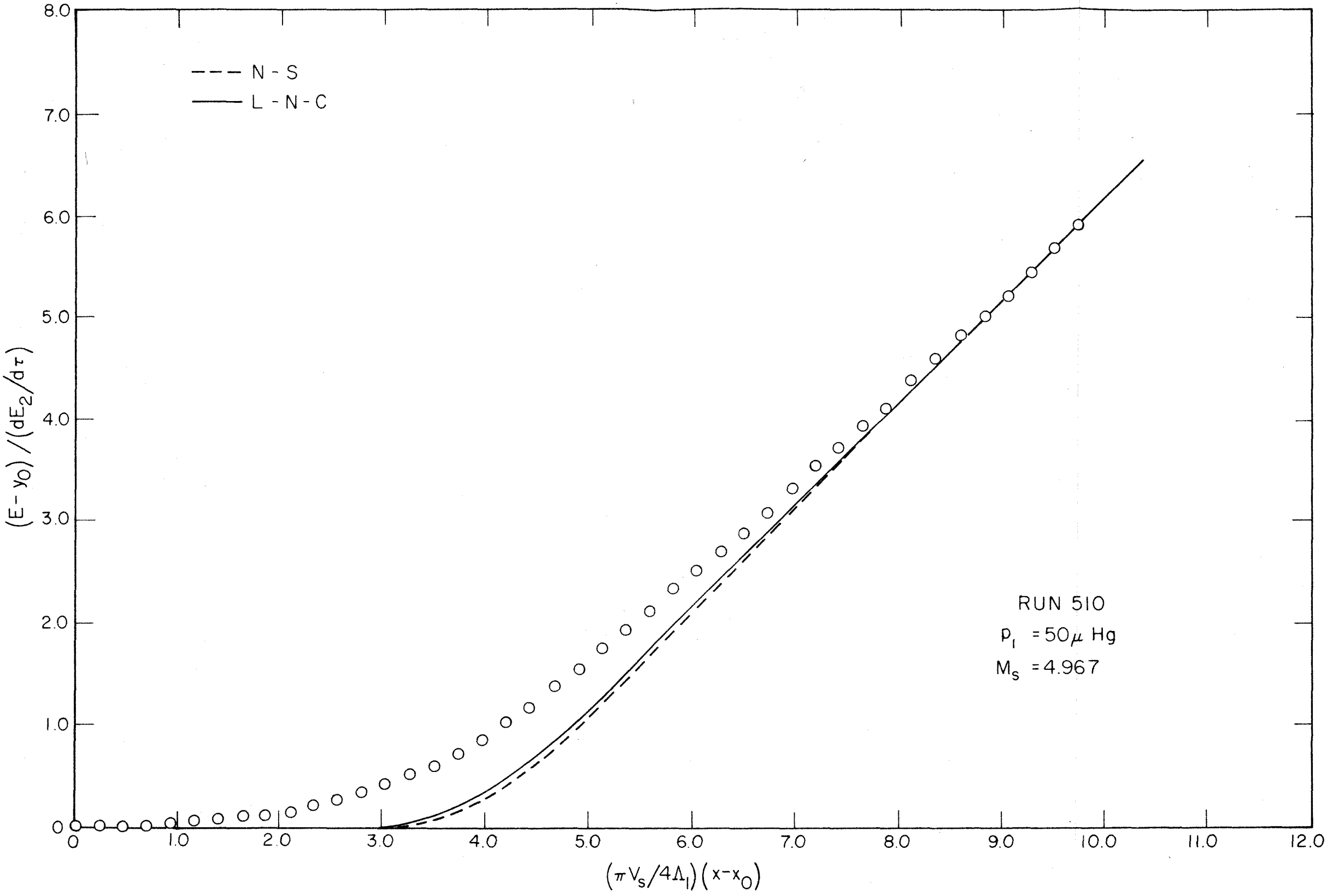
N - S
L - N - C
RUN 510
p_1 = 50μ Hg
M_s = 4.967
$(E - y_0) / (dE_2/d\tau)$
$(\pi V_s/4\Lambda_1)(x-x_0)$
0
1.0
2.0
3.0
4.0
5.0
6.0
7.0
8.0
9.0
10.0
11.0
12.0

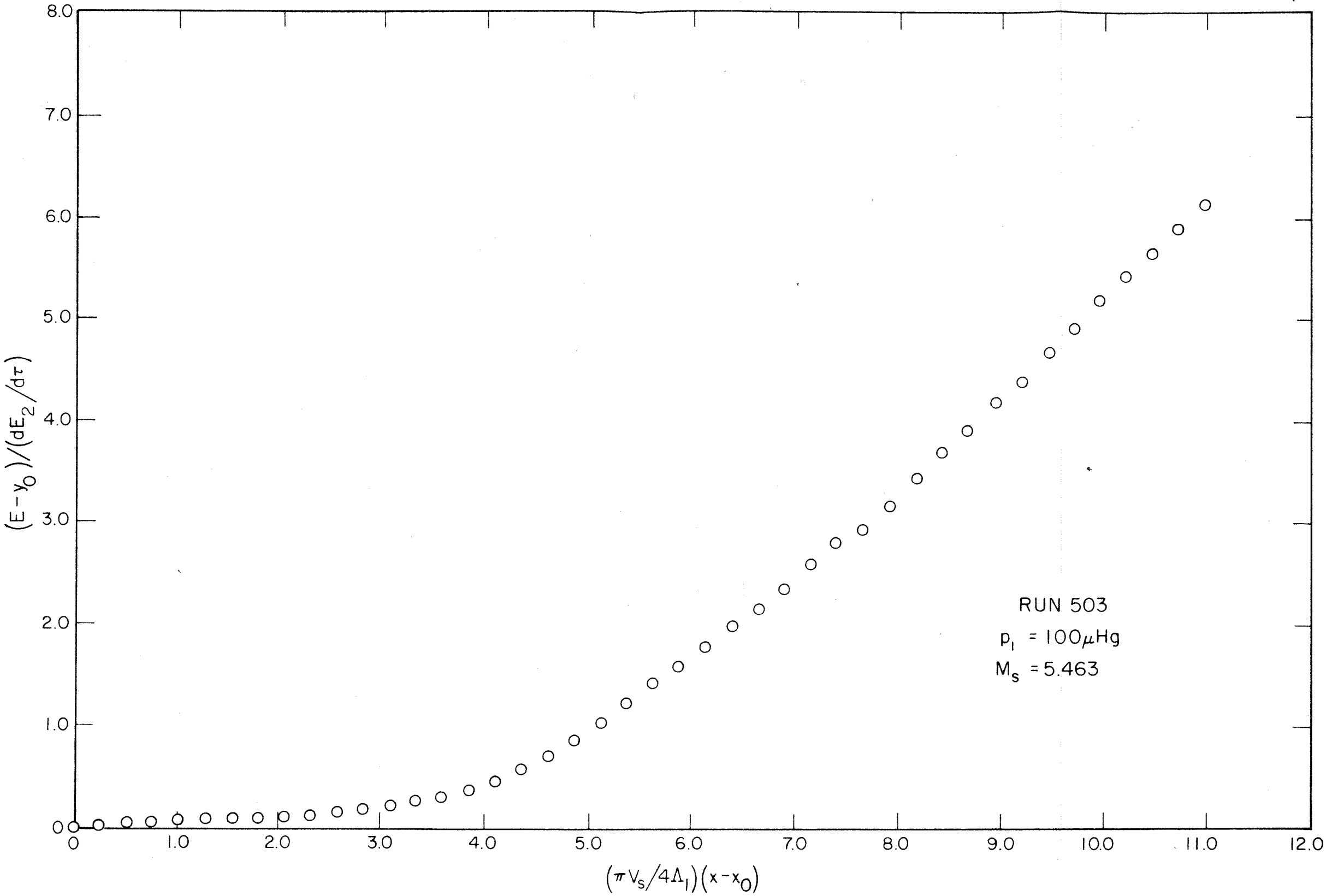
8.0
7.0
6.0
5.0
4.0
3.0
2.0
1.0
0
0
1.0
2.0
3.0
4.0
5.0
6.0
7.0
8.0
9.0
10.0
11.0
12.0
$(E-y_0)/(dE_2/d\tau)$
$(\pi V_s/4\Lambda_1)(x-x_0)$
RUN 503
p_1 = 100μHg
M_s = 5.463

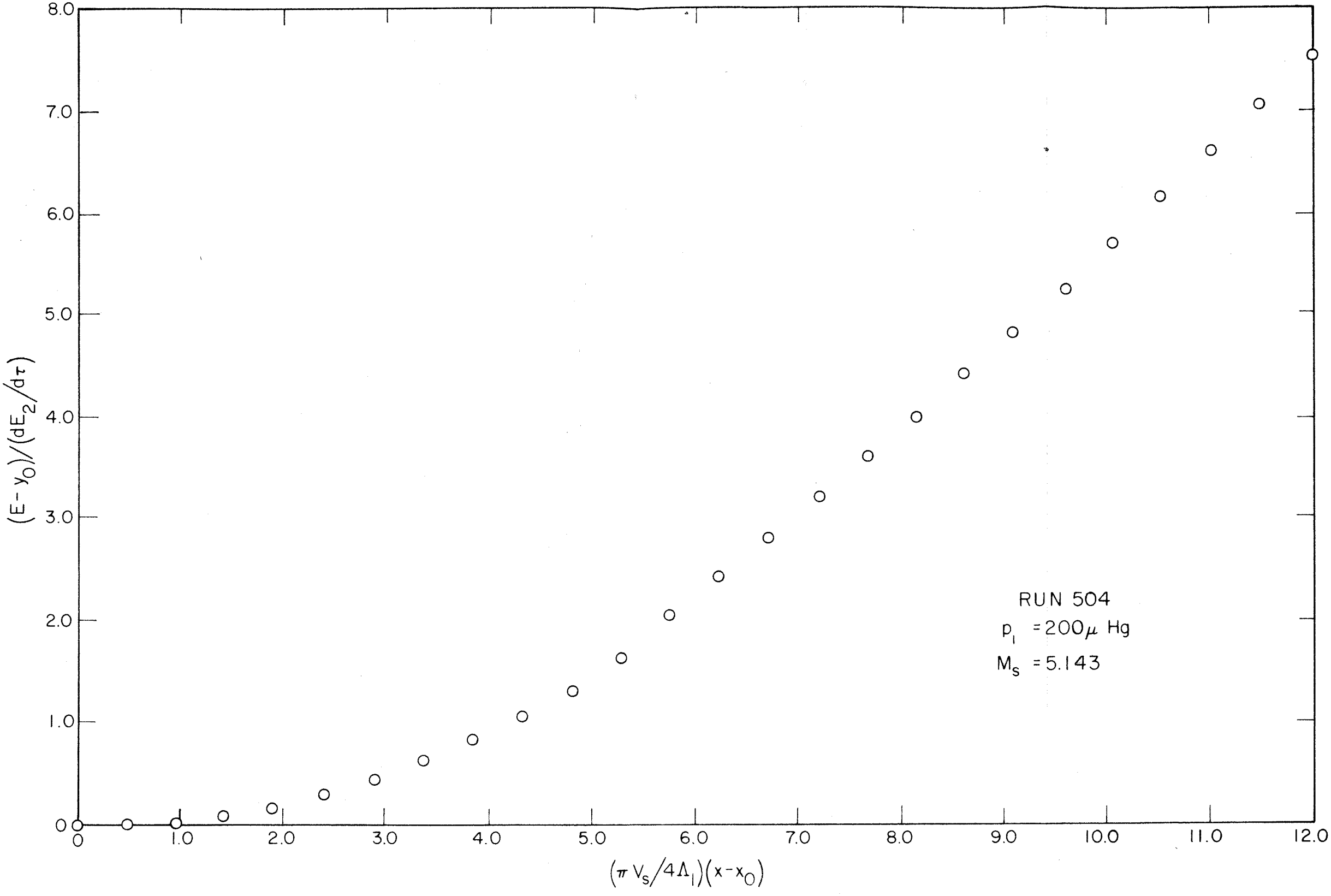
8.0
7.0
6.0
5.0
4.0
3.0
2.0
1.0
0
0
1.0
2.0
3.0
4.0
5.0
6.0
7.0
8.0
9.0
10.0
11.0
12.0
$(E-y_0)/(dE_2/d\tau)$
$(\pi V_s/4\Lambda_1)(x-x_0)$
RUN 504
p_1 = 200μ Hg
M_s = 5.143

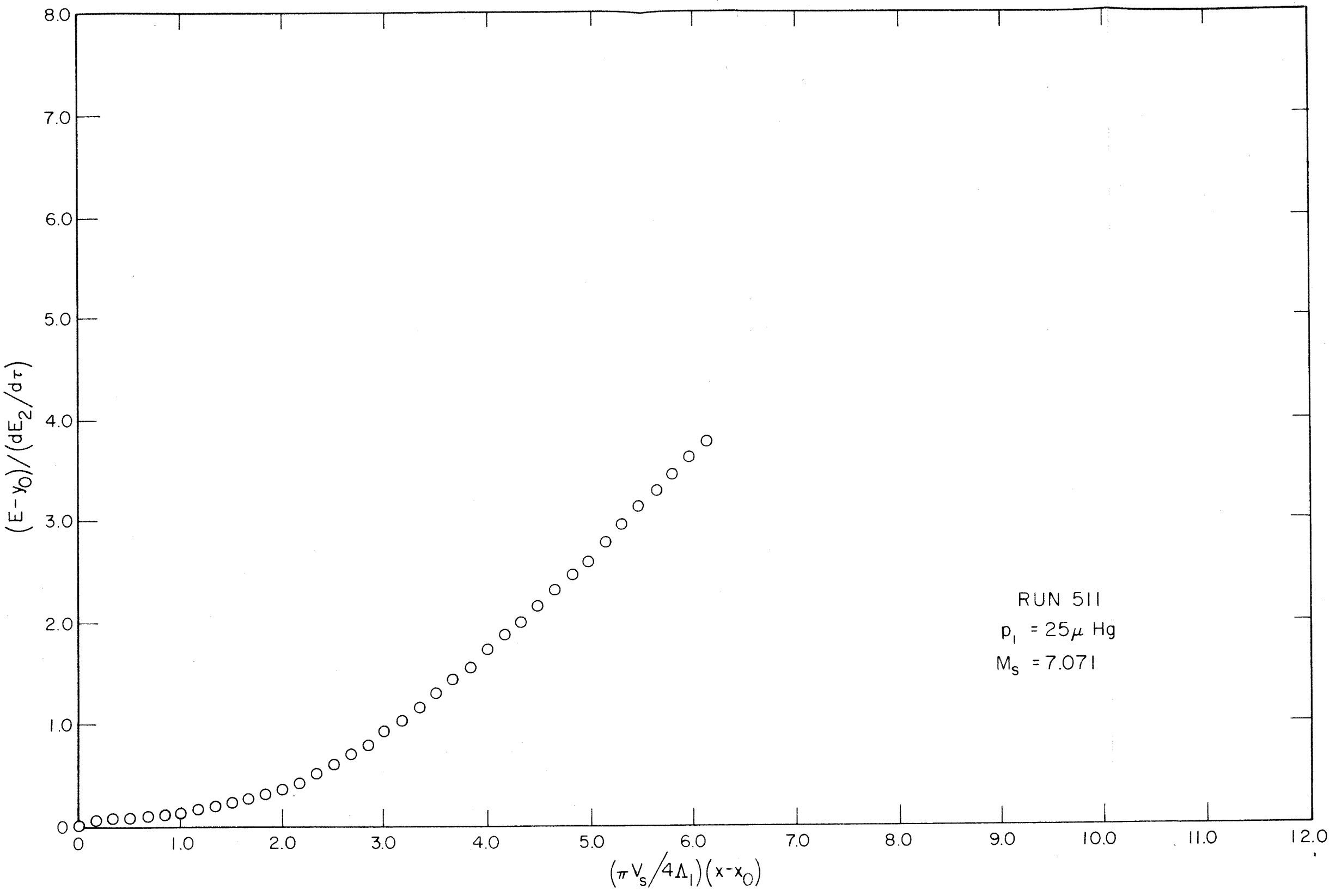
8.0
7.0
6.0
5.0
4.0
3.0
2.0
1.0
0
0
1.0
2.0
3.0
4.0
5.0
6.0
7.0
8.0
9.0
10.0
11.0
12.0
$(E-y_0)/(dE_2/d\tau)$
$(\pi V_s/4\Lambda_1)(x-x_0)$
RUN 511
p_1 = 25μ Hg
M_s = 7.071

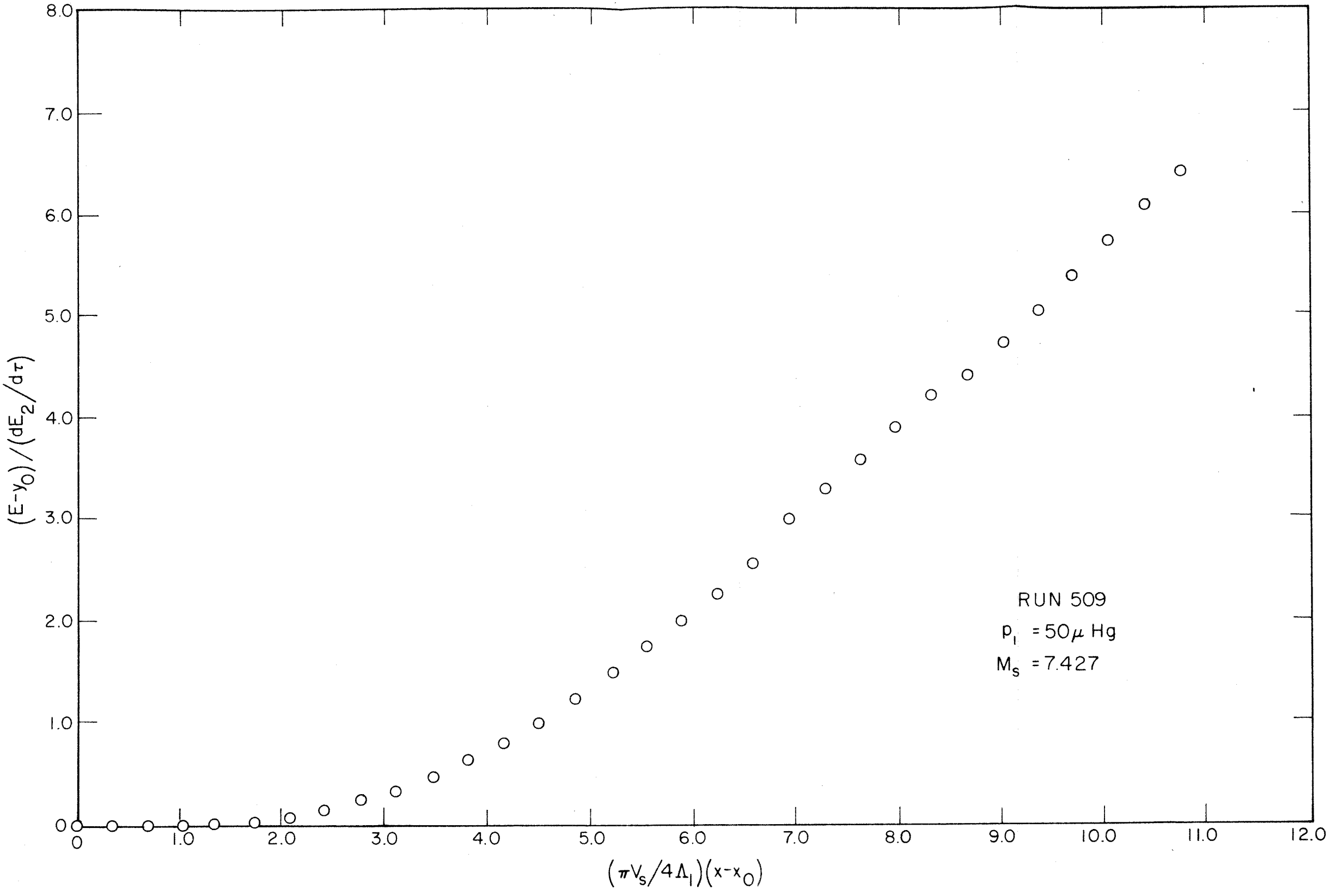
8.0
7.0
6.0
5.0
4.0
3.0
2.0
1.0
0
0
1.0
2.0
3.0
4.0
5.0
6.0
7.0
8.0
9.0
10.0
11.0
12.0
$(E-y_0)/(dE_2/d\tau)$
$(\pi V_s/4\Lambda_1)(x-x_0)$
RUN 509
p_1 = 50μ Hg
M_s = 7.427

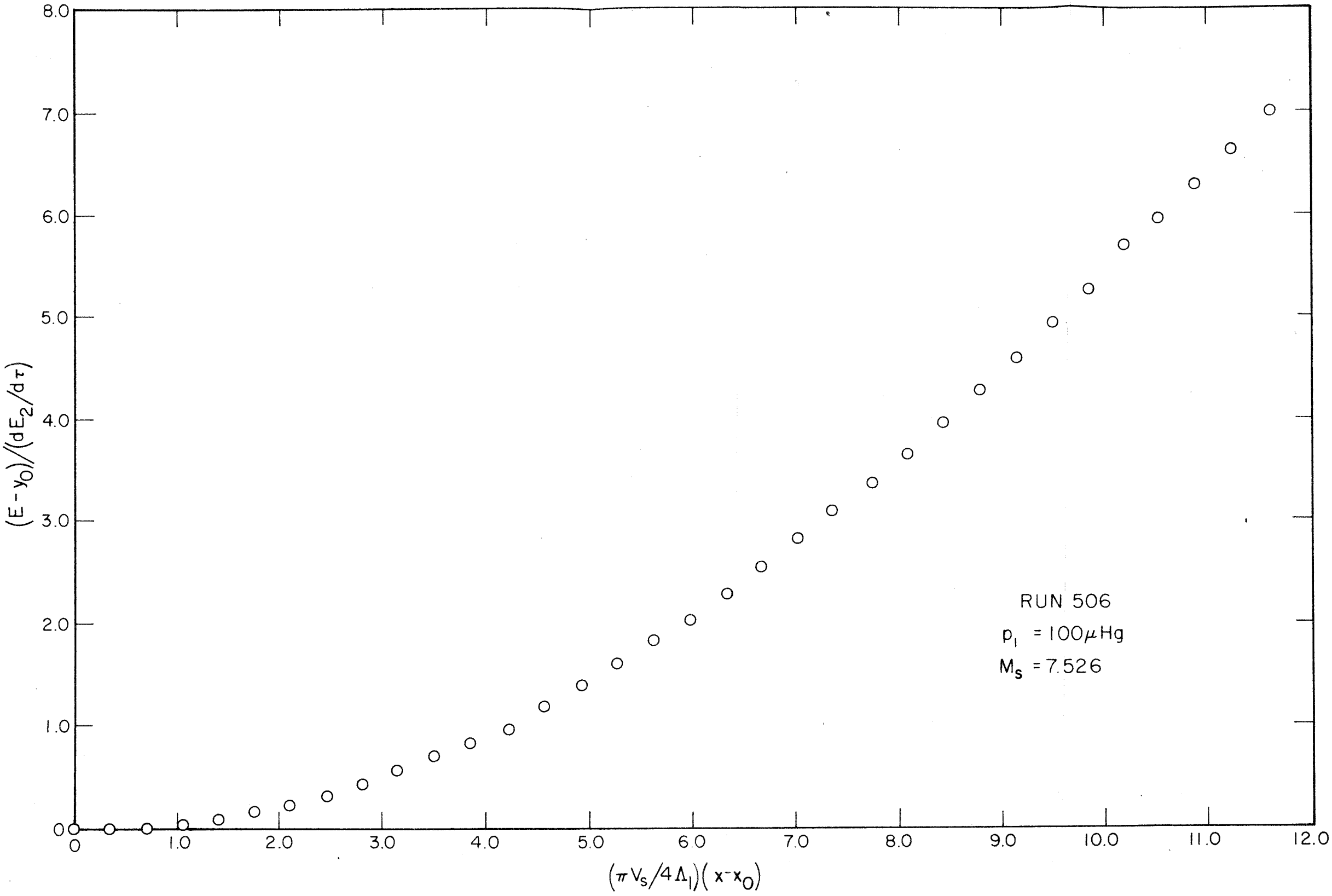
8.0
7.0
6.0
5.0
4.0
3.0
2.0
1.0
0
0
1.0
2.0
3.0
4.0
5.0
6.0
7.0
8.0
9.0
10.0
11.0
12.0
$(E-y_0)/(dE_2/d\tau)$
$(\pi V_s/4\Lambda_1)(x-x_0)$
RUN 506
p_1 = 100μHg
M_s = 7.526

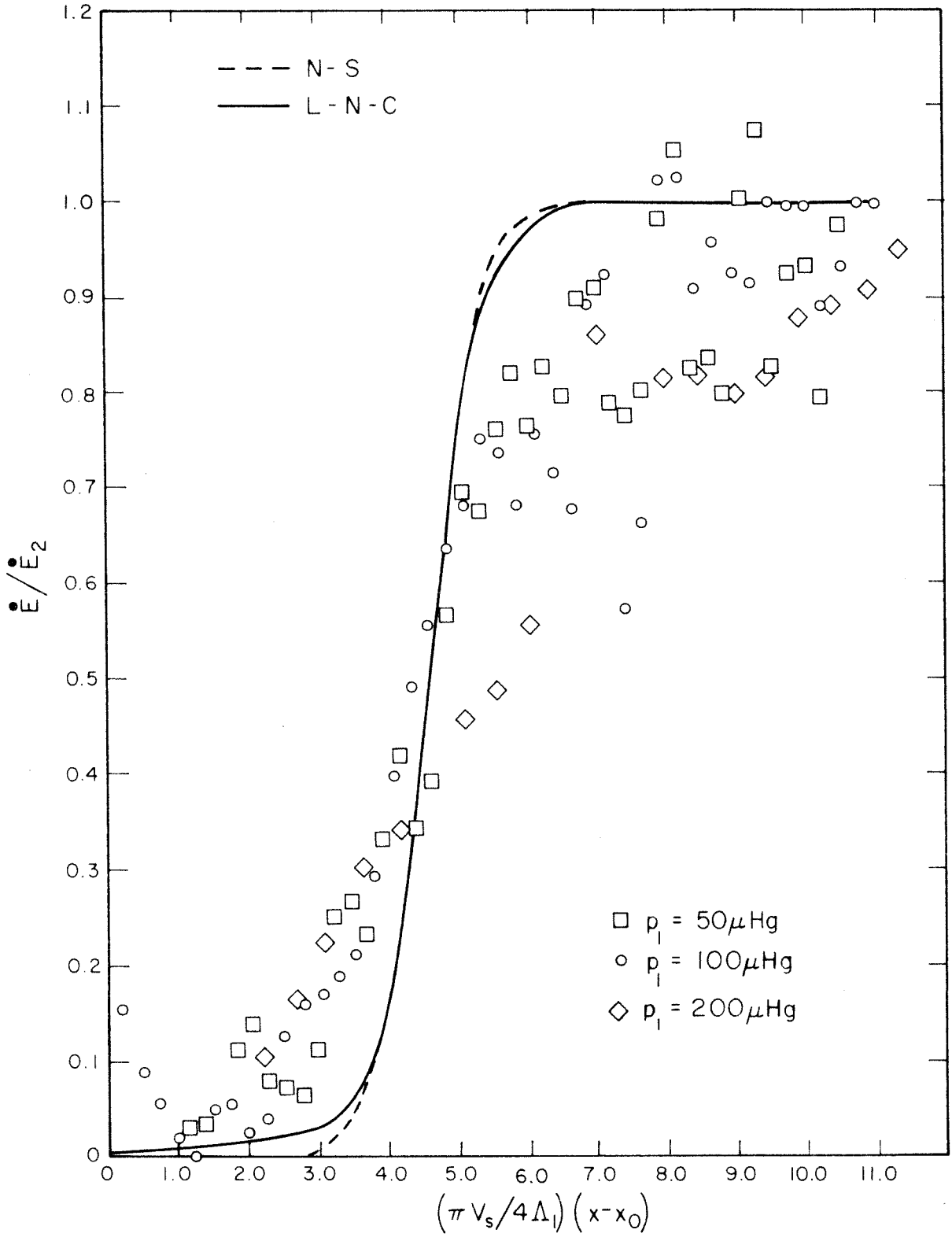

Fig. 16. $M_s \doteq 5$ Superimposed Differentiated Results

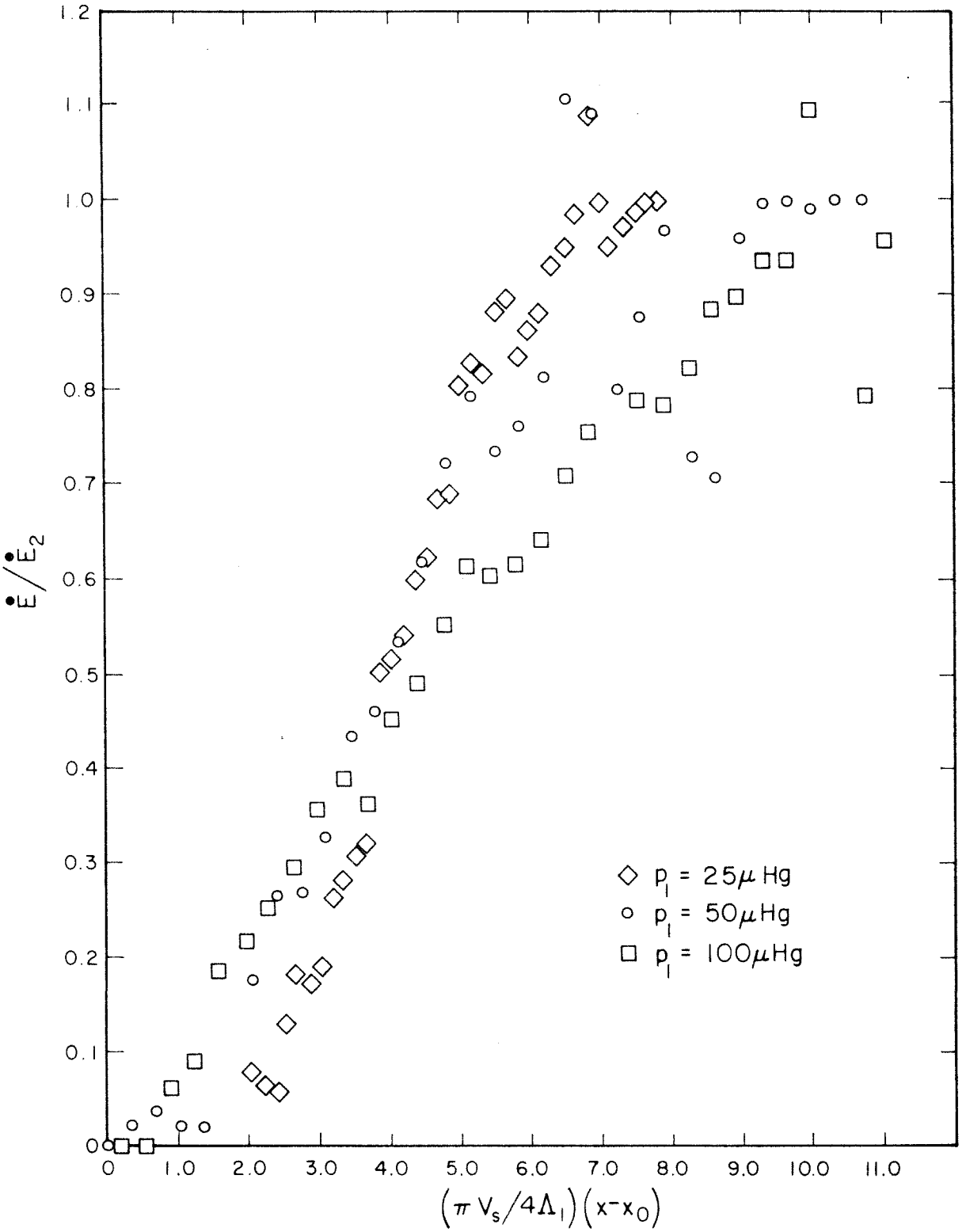

Fig. 17. $M_s \doteq 7.5$ Superimposed Differentiated Results

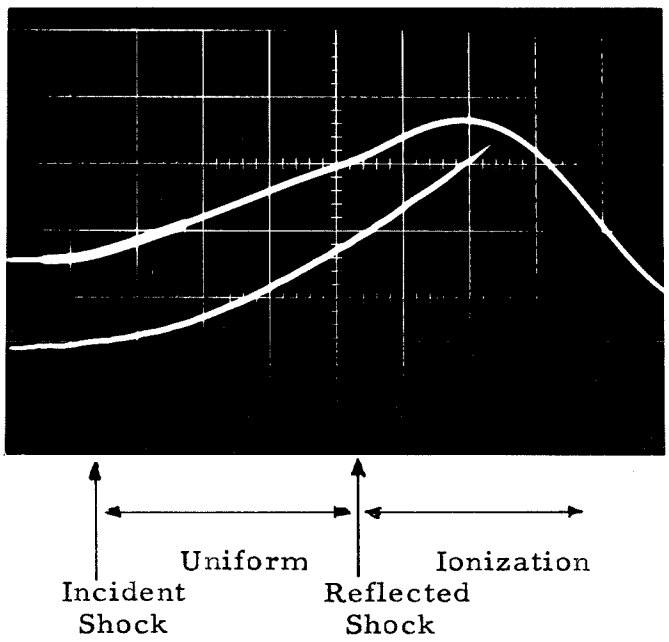

Upper: 5 mv/cm, 5 μsec/cm

Lower: .5 mv/cm, 1 μsec/cm

Reflected Shock Hits Wire Approx.

20 μsec After Incident Shock

Fig. 18. Ionization Effect

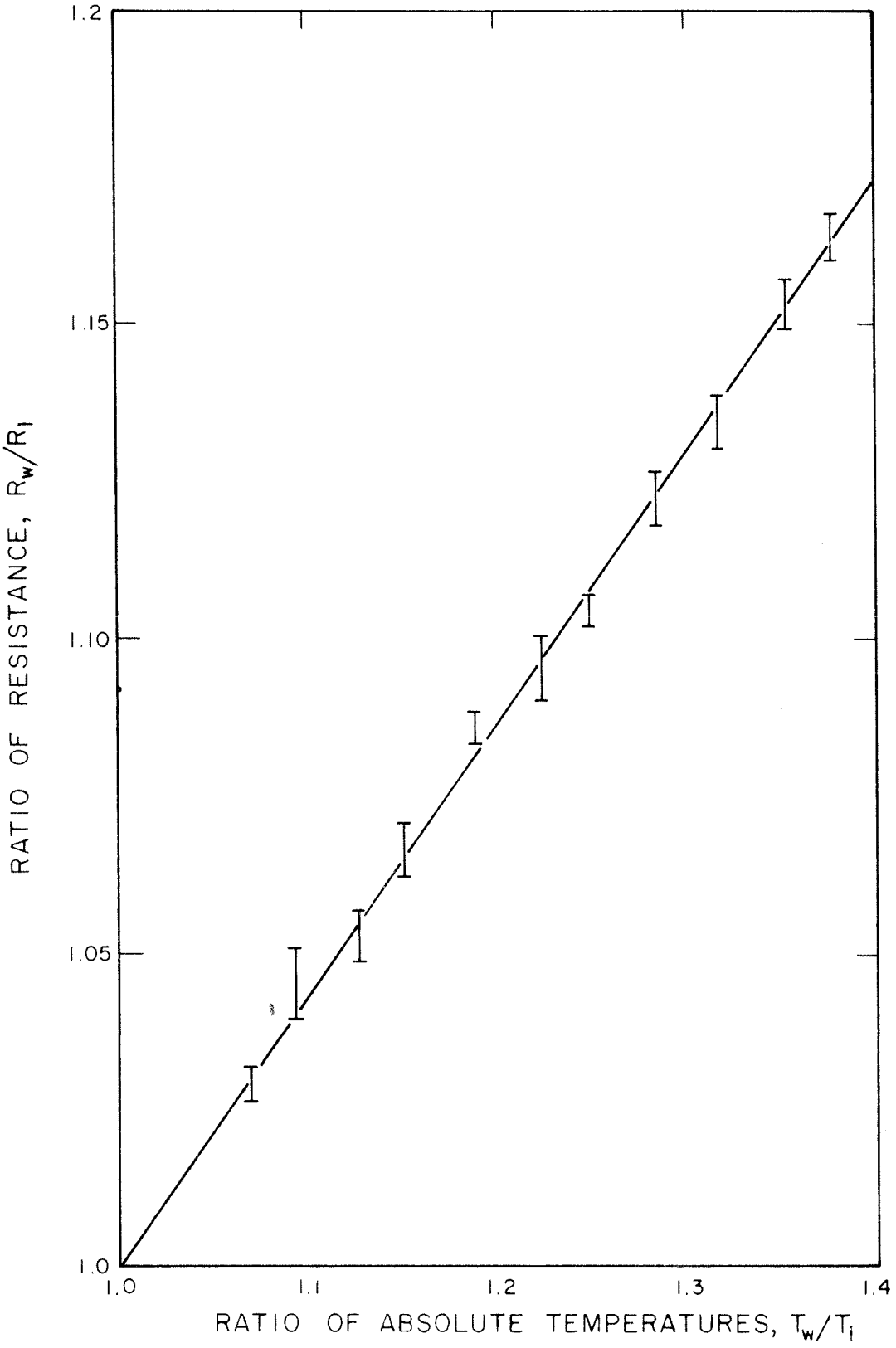

Fig. 19. α_1 Determination

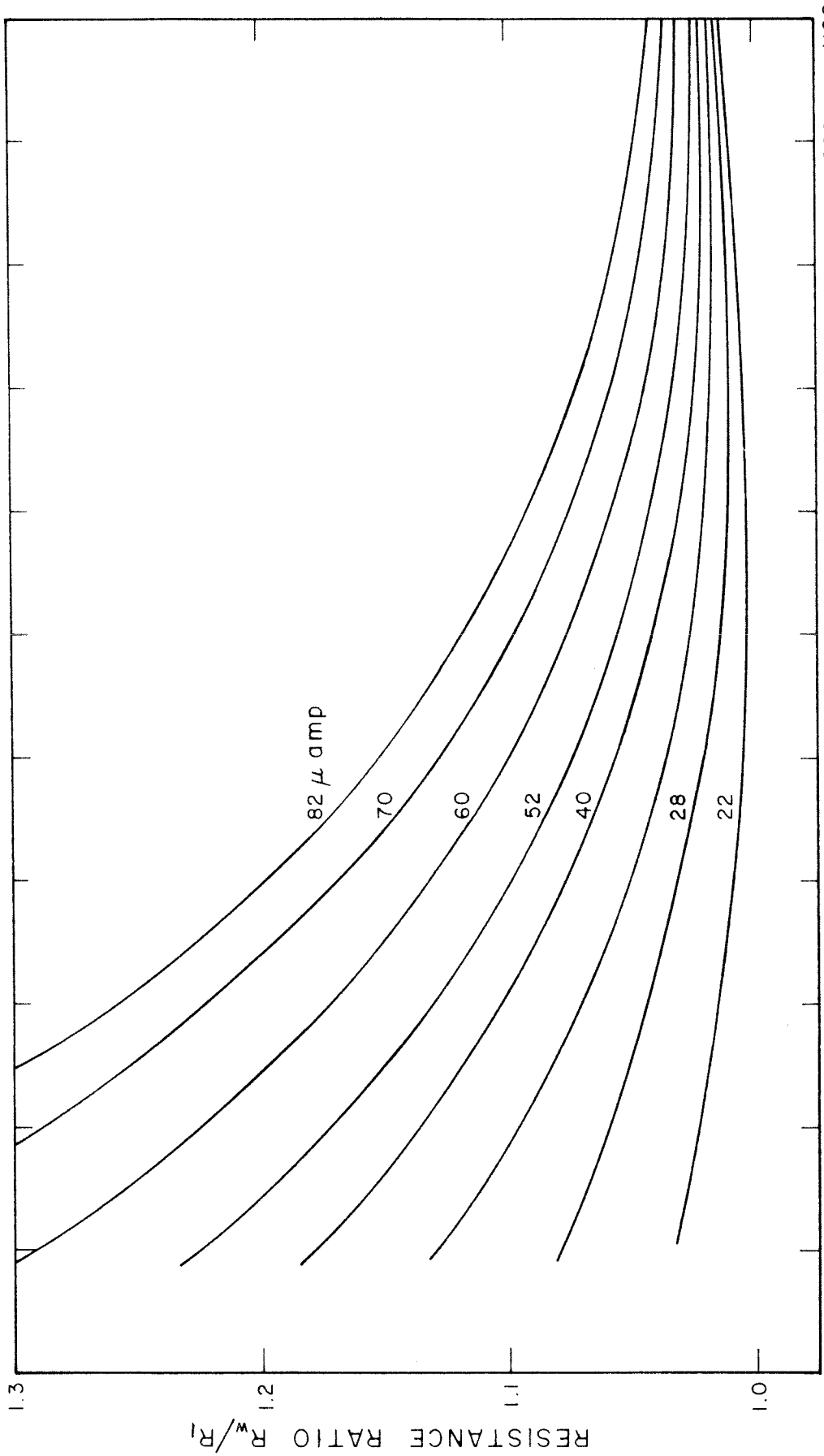

Fig. 20. p_1 Versus R_w for Values of Constant I

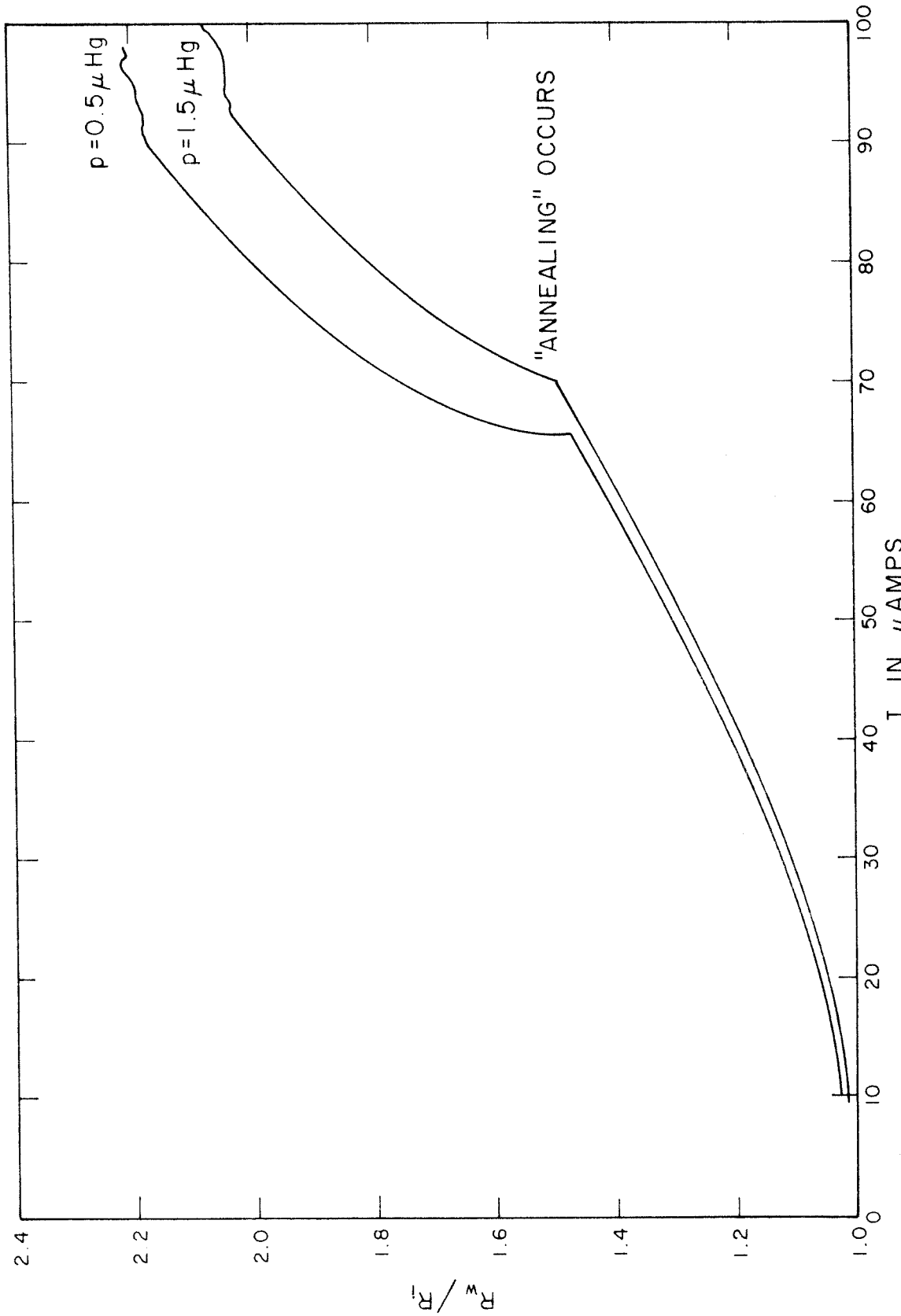

Fig. 21. Observation of Hysteresis Effect

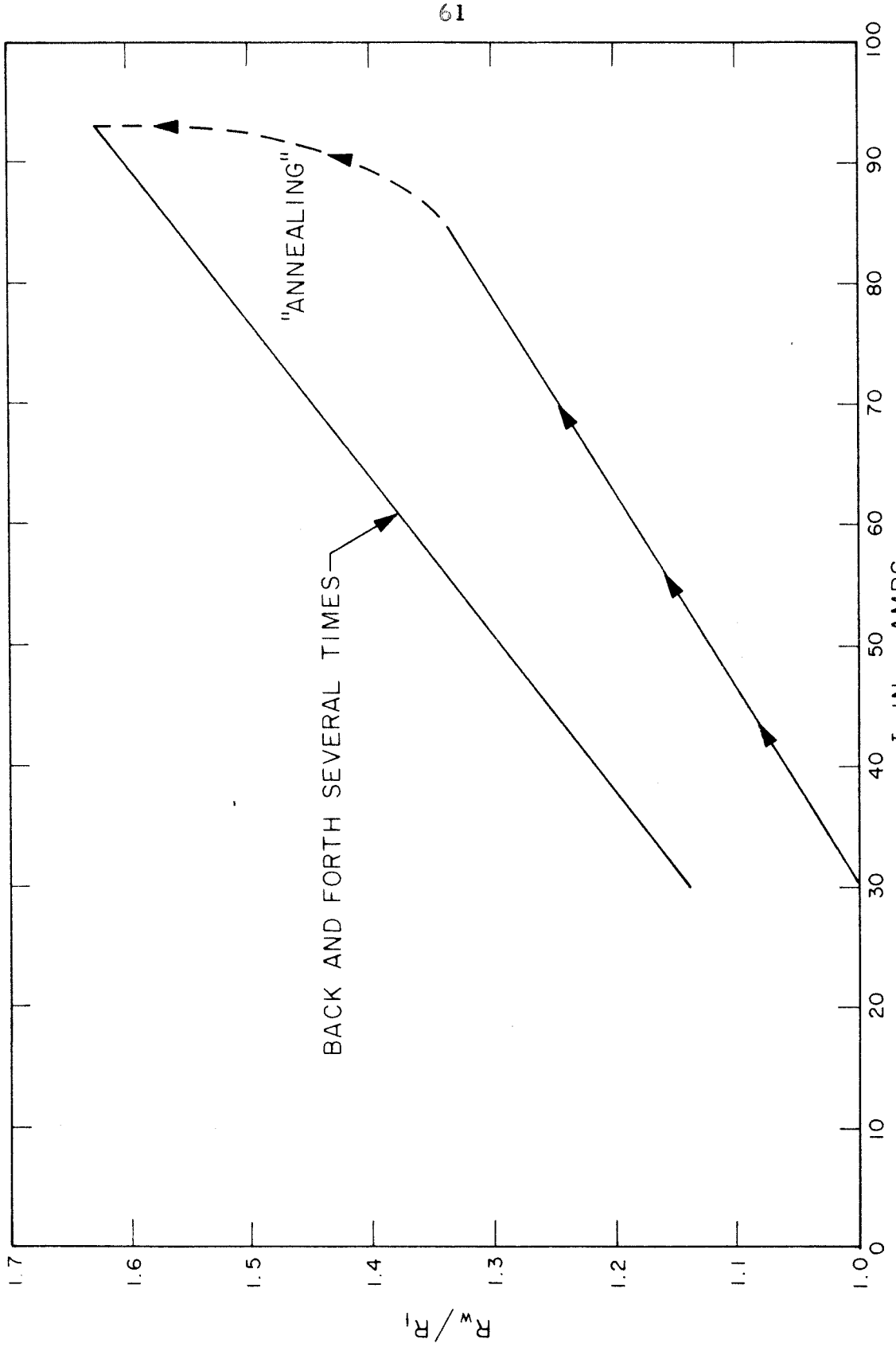

Fig. 22. Hysteresis Stability

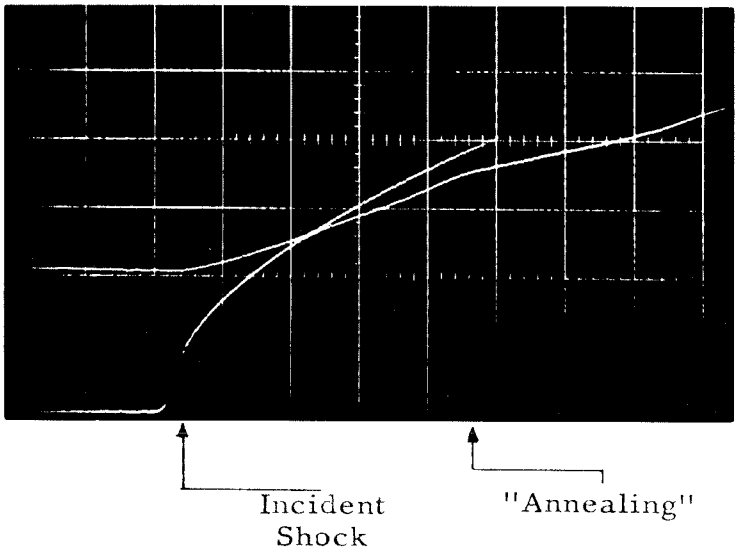

Upper: 10 mv/cm, 2 μsec/cm

Lower: 10 mv/cm, 2 μsec/cm

Lower Trace Is Coated Filament Response (Ref. 6)

Fig. 23. "Annealing" Effect During Run

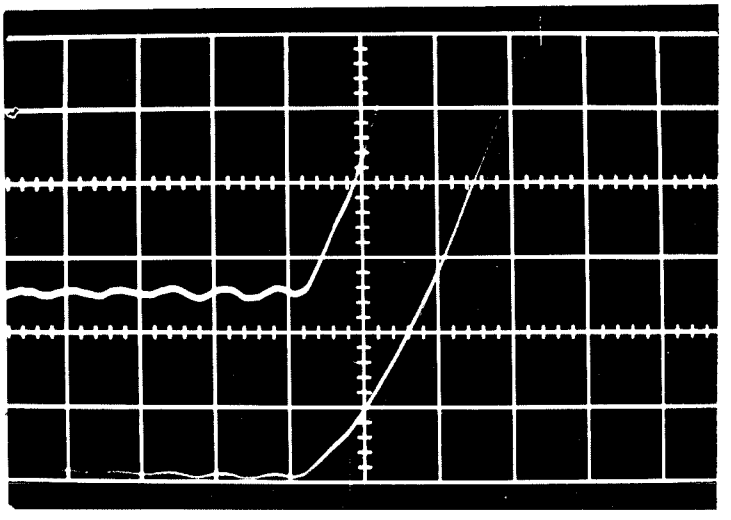

Upper: .5 mv/cm, 1 μ sec/cm (Wire 1)

Lower: 2 mv/cm, 1 μ sec/cm (Wire 2)

(At this pressure, shock structure duration should be approximately $\frac{1}{3}$ μ sec.)

Fig. 24. Strain Effect